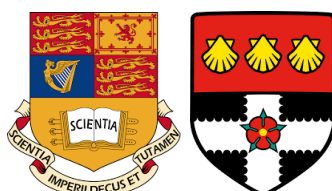

DISPERSION IN THE
NUMERICAL SOLUTION OF
LINEAR ADVECTION

AUTHOR:
GEORGIOS SIALOUNAS

SUPERVISOR:
DR TRISTAN PRYER



Report on NSDES
31 AUGUST, 2018

I confirm that this is my work and that it has not been submitted for a degree at another university or institution.

Georgios Sialounas

1 Error waves

The results and exposition in these chapters is largely from [1], [2] and [3]. In this section we will use a uniform grid in order to revise the Fourier argument. The grid is given by

$$x_n = nh, \quad n \in \mathbb{Z}. \quad (1)$$

We start by considering a central finite difference semi-discretization to the equation

$$u_t + u_x = 0, \quad (2)$$

given by

$$\frac{du_n}{dt} = -c \left(\frac{u_{n+1} - u_{n-1}}{2h} \right) \quad (3)$$

where

$$\{u_n(t)\} = \{U(x_n, t)\} \quad (4)$$

is the numerical solution on t -continuous lines (see [2, §1]). We will Fourier transform (3) to get

$$\hat{u}_{n+1} + 2i \left(\frac{\Omega h}{c} \right) \hat{u}_n - \hat{u}_{n-1} = 0. \quad (5)$$

We will now make use of the space shift operator

$$u_{n+1} = \mathbb{E}u_n \quad (6)$$

and of its image in the Fourier domain I am not sure how to get this

$$\hat{u}_{n+1} = \hat{E}(\Omega) \hat{u}_n \quad (7)$$

to turn (5) into

$$\left(\hat{E}^2 + 2i \left(\frac{\Omega h}{c} \right) \hat{E} - 1 \right) \hat{u}_n = 0. \quad (8)$$

We solutions for which $\hat{E}(\Omega)$ defined in (6) is independent of n . We do this by solving

$$\left(\hat{E}^2 + 2i \left(\frac{\Omega h}{c} \right) \hat{E} - 1 \right) = 0, \quad (9)$$

which gives

$$\hat{E}_1 = -i \left(\frac{\Omega h}{c} \right) + \sqrt{1 - \left(\frac{\Omega h}{c} \right)^2} \quad (10)$$

$$\hat{E}_2 = -i \left(\frac{\Omega h}{c} \right) - \sqrt{1 - \left(\frac{\Omega h}{c} \right)^2} \quad (11)$$

In [2], these values of \hat{E} are called characteristic ratios. Briefly, we can express solutions of (3) as

$$\{u_n(t)\} = \{p_n(t)\} + \{q_n(t)\}, \quad (12)$$

where p_n and q_n are two different fundamental types of solutions. Their Fourier transforms are given by

$$\hat{p}_n = \hat{p}_0(\Omega) \left[\hat{E}_1 \right]^n \quad \text{and} \quad (13)$$

$$\hat{q}_n = \hat{q}_0(\Omega) \left[\hat{E}_2 \right]^n \quad (14)$$

$$(15)$$

and the presence of the respective \hat{E} in each expression indicates that they will have different propagation properties. In the context of the parasite investigation this is extremely important.

In particular, as [3] show, each ratio relates to components of the solution which travel at different group velocities. Although we explore this phenomenon at greater depth in the sections that follow, for the time being its is sufficient to say that when the mesh is not uniform the two types of solutions may correspond to components of the solution which travel in opposite directions.

It is also worth noting what happens when $\Omega h/c$ is less than, equal to or greater than 1 in (10)-(11):

- $\Omega h/c \leq 1$: In this case $|\hat{E}_{1,2}| = 1$ and solutions of type p_n and q_n will propagate at group velocities given by [2, §8: (68)-(69)] with constant amplitude.
- $\Omega h/c > 1$: In this case, as [4] and [2, §4] show, the numerical solutions to (3) will decay in amplitude with x for \hat{E}_1 and with $-x$ for \hat{E}_2 . Incidentally, for this reason - i.e. because the amplitude of sinusoidal solutions to (3) will decay for Ω greater than this frequency - the frequency $\Omega_c = c/h$ is called the cut-off frequency.

Now, consider the case when we replace the uniform grid in (1) with an irregular one. Consider, for example, a grid which has spacing $h/2$ in its first half and $2h$ everywhere else (see Fig.2). In this example, $x \in [0, 2]$, $h(x \leq 1) = 0.05$ and $h(x > 1) = 0.1$.

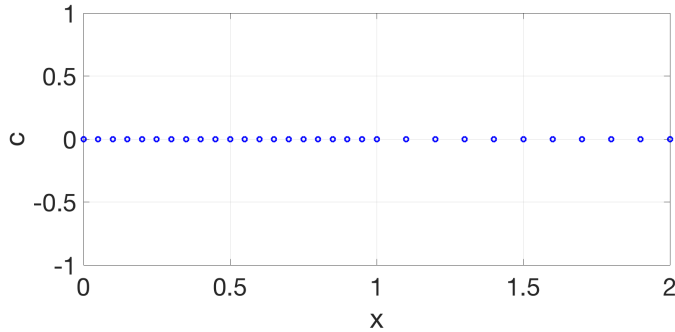


Figure 2: A sample grid where where the two halves of the domain have different resolution.

In this case, when a (smooth) solution crosses over from one region of the grid to the other, a parasite will be emitted from the location of the grid discontinuity. The parasite is a spurious, highly (spatially) oscillatory wave which, for certain values of $\Omega h/c$ will travel in the opposite direction from that of the physical solution. The parasite is examined in detail in a range of works by Vichnevetsky and others: [5], [3] [6] and more recently by [7] and[8] to name but a few. I go into more depth on this in my other report so I'll stop here for now.

1.1 Parasites-an alternative view poin

For the time being, I would like to provide another avenue for exploring parasites which is from [1]. In that paper, Vichnevetsky and Peiffer say that when we try to approximate hyperbolic PDEs with FD or FEM we introduce errors in the characteristic velocities of these equations (by that I assume they mean the velocities at which characteristics travel). In the analysis and numerical models we used so far we did a lot of work with both step and smooth initial conditions. In particular, for smooth ICs they ([1]) say that group velocity of the sinusoidal components which are summed up to give the solution is frequency dependent.

It is in this frequency that the errors manifest in, causing sinusoidal components of different frequencies to propagate at different group velocities. This behaviour is unphysical i.e. it manifests in the numerical solution but NOT in the actual PDE solution. These errors, which manifest as spurious dispersion phenomena are most readily observed when there is some sharp spatial variation in either the initial conditions or the grid spacing or something else. Their wavelength will be near $2\Delta x$, something which we observed to and something which is shown in both [1] and [2].

The paper gives details about both FD and FEM discretization but since we started with FD we'll continue with that. What we'll try to do is say something about the short-wavelength spurious oscillations that Trefethen (and us too) call parasites from an NSDEs perspective rather than with a Fourier argument. The only thing I'll do here is go through the work in [1, §3] and explain the content of [2, §2: Property 1]. We'll start by rewriting (3) using u_n for the value of the numerical solution at even-numbered grid-points and v_n for odd-numbered grid-points:

$$\alpha \frac{du_n}{dt} + \left(\frac{1-\alpha}{2} \right) \left(\frac{dv_{n+1}}{dt} + \left(\frac{dv_{n-1}}{dt} \right) = -c \left(\frac{v_{n+1} - v_{n-1}}{2h} \right) \quad (16)$$

for even n and

$$\alpha \frac{dv_n}{dt} + \left(\frac{1-\alpha}{2} \right) \left(\frac{du_{n+1}}{dt} + \frac{du_{n-1}}{dt} \right) = -c \left(\frac{u_{n+1} - u_{n-1}}{2h} \right) \quad (17)$$

for odd n . The reason for using the α is to enable the analysis for both FEM and FD to be done in one go, since the RHS will be the same for both and a suitable choice of α will give either one or the other scheme ($\alpha = 1$ gives FD and $\alpha = 2/3$ gives FEM). Now, as is mentioned in [2, §2: Property 1] this is a consistent approximation to the system of equations given by

$$\begin{aligned} \alpha \frac{\partial u}{\partial t} + (1-\alpha) \frac{\partial v}{\partial t} &= -c \frac{\partial v}{\partial x} \\ (1-\alpha) \frac{\partial v}{\partial t} + \alpha \frac{\partial u}{\partial t} &= -c \frac{\partial u}{\partial x} \end{aligned} \quad (18)$$

where u and v are smooth functions of x and t

2 Interpolant

The interpolant $\mathcal{I}U$ is a piecewise bi-linear function in x and t . In order to define the interpolant we first define the numerical solution

$$U_j^i, \quad 1 \leq i \leq N_t, 1 \leq j \leq N_x \quad (19)$$

where N_t and N_x are the number of time-steps and grid-points respectively. We define $\mathcal{I}U(t, x)$ in the time-space patches $D_{i,j} := [t_{i-1}, t_i] \times [x_{j-1}, x_j]$ such that $(t, x) \in D_{i,j}$:

$$\mathcal{I}U(t, x) := \frac{t - t_{i-1}}{\Delta t} \left(\frac{x - x_{j-1}}{\Delta x} U_j^i + \frac{x_j - x}{\Delta x} U_{j-1}^i \right) + \frac{t_i - t}{\Delta t} \left(\frac{x - x_{j-1}}{\Delta x} U_j^{i-1} + \frac{x_j - x}{\Delta x} U_{j-1}^{i-1} \right). \quad (20)$$

We can differentiate (20) to obtain expressions for $\mathcal{I}U_x$ and $\mathcal{I}U_t$:

$$\begin{aligned}\mathcal{I}U_t(t, x) &:= \frac{1}{\Delta t} \left(\frac{x - x_{j-1}}{\Delta x} U_j^i + \frac{x_j - x}{\Delta x} U_{j-1}^i \right) - \frac{1}{\Delta t} \left(\frac{x - x_{j-1}}{\Delta x} U_j^{i-1} - \frac{x_j - x}{\Delta x} U_{j-1}^{i-1} \right), \\ \mathcal{I}U_x(t, x) &:= \frac{t - t_{i-1}}{\Delta t} \left(\frac{1}{\Delta x} U_j^i - \frac{1}{\Delta x} U_{j-1}^i \right) + \frac{t_i - t}{\Delta t} \left(\frac{1}{\Delta x} U_j^{i-1} - \frac{1}{\Delta x} U_{j-1}^{i-1} \right).\end{aligned}\quad (22)$$

These expressions will be piecewise constant in the variable we differentiated (20) to get them and linear in the other. The implication is that they will be discontinuous at grid-points: t_i for $\mathcal{I}U_t(t_i, x)$ and x_j for $\mathcal{I}U_x(t, x_j)$.

This is a problem only for a linear interpolant. If we use a quadratic (or higher order) interpolant this will no longer be an issue. However, since we will use a linear interpolant for now, we will approximate (21)-(22) at the mid-points of the time-space patches, where the interpolant's derivatives are well defined:

$$(t_{i-1/2}, x_{j-1/2}) = \left(\frac{t_{i-1} + t_i}{2}, \frac{x_{j-1} + x_j}{2} \right). \quad (23)$$

If we substitute (23) for (t, x) in (21)-(22) we get

$$\mathcal{I}U_t(t_{i-1/2}, x_{j-1/2}) = \frac{1}{2} \left(\frac{U_j^i - U_j^{i-1}}{\Delta t} \right) + \frac{1}{2} \left(\frac{U_{j-1}^i - U_{j-1}^{i-1}}{\Delta t} \right) \quad (24)$$

$$\mathcal{I}U_x(t_{i-1/2}, x_{j-1/2}) = \frac{1}{2} \left(\frac{U_j^i - U_{j-1}^i}{\Delta x} \right) + \frac{1}{2} \left(\frac{U_j^{i-1} - U_{j-1}^{i-1}}{\Delta x} \right) \quad (25)$$

3 Bound

Consider

$$u_t + u_x = 0$$

$$v_t + v_x = R$$

with error given by

$$e = u - v \quad (26)$$

The bound for the error in a domain $(0, L) \times (0, t)$ is given by

$$\|e(t)\|_{L^2} \leq \left[\exp(t) \left(\|e(0)\|_{L^2}^2 + \int_0^t \|R(s)\|_{L^2}^2 \exp(-s) ds \right) \right]^{1/2}, \quad (27)$$

where $R(t, x)$ is given by

$$-R(t, x) = \mathcal{I}U_t(t, x) + \mathcal{I}U_x(t, x). \quad (28)$$

Hence, $R(t, x)$ is a bilinear function in t and x . Furthermore, it is discontinuous at points (t_i, x_j) due to the discontinuity of $\mathcal{I}U_t$ and $\mathcal{I}U_x$ respectively at those points. For this reason, when we go about calculating the bound in (27), we evaluate R at the midpoints of the time-space patches, as in (24)-(25).

4 Integration

We want to calculate the RHS of (27), for which we have to integrate $R(t, x)$ in space and time. Since we will be using a linear interpolant for $\mathcal{I}U$ we will just use the midpoint rule. In the future we will use Gauss quadrature. We calculate the expression as follows, assuming $e_0 \equiv 0$:

$$\int_0^t \|R(s)\|_{L^2}^2 \exp(-s) ds \approx \sum_{i=1}^{N_t} \Delta t \left(\sum_{j=1}^{N_x} \Delta x (R(t_{i-1/2}, x_{j-1/2}))^2 \right), \quad (29)$$

where

$$-R(t_{i-1/2}, x_{j-1/2}) = \mathcal{I}U_t(t_{i-1/2}, x_{j-1/2}) + \mathcal{I}U_x(t_{i-1/2}, x_{j-1/2}). \quad (30)$$

The expressions for the RHS in (30) are given in (24)-(25).

5 Order of convergence

In this section we will look at how the quantity

$$\int_0^T \|u(\cdot) - \mathcal{I}U(\cdot)\|_{L^2(0,L)} ds \quad (31)$$

should converge. Note that we will couple dt to dx . We begin by considering the order of the quantity

$$u_x(t_{i-1/2}, x_{j-1/2}) - \mathcal{I}U_x(t_{i-1/2}, x_{j-1/2}). \quad (32)$$

In order to find the order of convergence we will substitute the exact solution for u_x in the right-hand side of (25). We will then Taylor expand the terms in the rhs of (25) about $(t_{i-1/2}, x_{j-1/2})$ and substitute this back in (25). Let us look at each of the terms in turn. Note that in the equation that follow, for brevity, whenever we avoid

specifying where u and its derivatives are evaluated, the evaluation point will be at $(t_{i-1/2}, x_{j-1/2})$.

$$\begin{aligned} u(t_i, x_j) &= u + \left(\frac{\Delta t}{2} \partial_t + \frac{\Delta x}{2} \partial_x \right) u + \frac{1}{2} \left(\frac{\Delta t}{2} \partial_t + \frac{\Delta x}{2} \partial_x \right)^2 u \\ &\quad + \frac{1}{3!} \left(\frac{\Delta t}{2} \partial_t + \frac{\Delta x}{2} \partial_x \right)^3 u + \mathcal{O}((\Delta t + \Delta x)^4) \end{aligned} \quad (33)$$

$$\begin{aligned} u(t_i, x_{j-1}) &= u + \left(\frac{\Delta t}{2} \partial_t - \frac{\Delta x}{2} \partial_x \right) u + \frac{1}{2} \left(\frac{\Delta t}{2} \partial_t - \frac{\Delta x}{2} \partial_x \right)^2 u \\ &\quad + \frac{1}{3!} \left(\frac{\Delta t}{2} \partial_t - \frac{\Delta x}{2} \partial_x \right)^3 u + \mathcal{O}((\Delta t + \Delta x)^4) \end{aligned} \quad (34)$$

$$\begin{aligned} u(t_{i-1}, x_j) &= u + \left(-\frac{\Delta t}{2} \partial_t + \frac{\Delta x}{2} \partial_x \right) u + \frac{1}{2} \left(-\frac{\Delta t}{2} \partial_t + \frac{\Delta x}{2} \partial_x \right)^2 u \\ &\quad + \frac{1}{3!} \left(-\frac{\Delta t}{2} \partial_t + \frac{\Delta x}{2} \partial_x \right)^3 u + \mathcal{O}((\Delta t + \Delta x)^4) \end{aligned} \quad (35)$$

$$\begin{aligned} u(t_{i-1}, x_{j-1}) &= u + \left(-\frac{\Delta t}{2} \partial_t - \frac{\Delta x}{2} \partial_x \right) u + \frac{1}{2} \left(-\frac{\Delta t}{2} \partial_t - \frac{\Delta x}{2} \partial_x \right)^2 u \\ &\quad + \frac{1}{3!} \left(-\frac{\Delta t}{2} \partial_t - \frac{\Delta x}{2} \partial_x \right)^3 u + \mathcal{O}((\Delta t + \Delta x)^4). \end{aligned} \quad (36)$$

We now substitute (33)-(36) in (24) and (25) and simplify to obtain

$$u_t - \mathcal{I}u_t = \frac{1}{2\Delta t} \left[2 \left(\frac{\Delta t}{2} \right) \left(\frac{\Delta x}{2} \right)^2 \partial_t \partial_{xx} u + \frac{2}{3} \left(\frac{\Delta t}{2} \right)^3 \partial_{ttt} u + h.o.t. \right] = \mathcal{O}(\Delta x^2) \text{ and} \quad (37)$$

$$u_x - \mathcal{I}u_x = \frac{1}{2\Delta x} \left[2 \left(\frac{\Delta t}{2} \right)^2 \left(\frac{\Delta x}{2} \right) \partial_{tt} \partial_x u + \frac{2}{3} \left(\frac{\Delta x}{2} \right)^3 \partial_{xxx} u + h.o.t. \right] = \mathcal{O}(\Delta x^2). \quad (38)$$

Note that in our simulations we have used the fact that we coupled dt to dx^2 . This implies that terms involving dt^2 are higher than order 2, which is why we don't include them in the leading order term in the rhs of the equations above. Essentially, we can see that the leading order term is $\mathcal{O}(\Delta x^2)$. Most importantly, we can use (37) and (32) to show that the quantity

$$\mathcal{I}U_t + \mathcal{I}U_x \quad (39)$$

should be expected to converge with order 2 for a uniform mesh with smooth initial conditions. Indeed, this is confirmed in practice as we will see in Figures 4 and 5.

6 Numerical results

What is the right order of convergence of the bound? Let's look at the individual components. In order to make this a complete investigation we will look at both smooth and discontinuous initial conditions. The smooth initial conditions will be given by

$$u_0(x) = \exp(-10(x - k)^2), \quad (40)$$

with $k \in [0, L]$ while the step initial conditions will be given by

$$u_0(x) = \begin{cases} 1 & \text{if } x \in [k - \varepsilon, k + \varepsilon] \\ 0 & \text{otherwise,} \end{cases} \quad (41)$$

with $k \in [0, L]$ and $\varepsilon \in (0, L/2]$.

6.1 $u_{x,t} - \mathcal{I}U_{x,t}$ -uniform grid

In this section we are trying to calculate the order of convergence of $u_{x,t} - \mathcal{I}U_{x,t}$ for a uniform grid. Here, by $u_{x,t}$ I mean differentiation wrt to one independent variable at a time. As an exact solution we use

$$u(x, t) = \exp(-10(x - 8 - t)^2) \quad (42)$$

for which

$$u_x = -20(x - 8 - t) \exp(-10(x - 8 - t)^2) \quad (43)$$

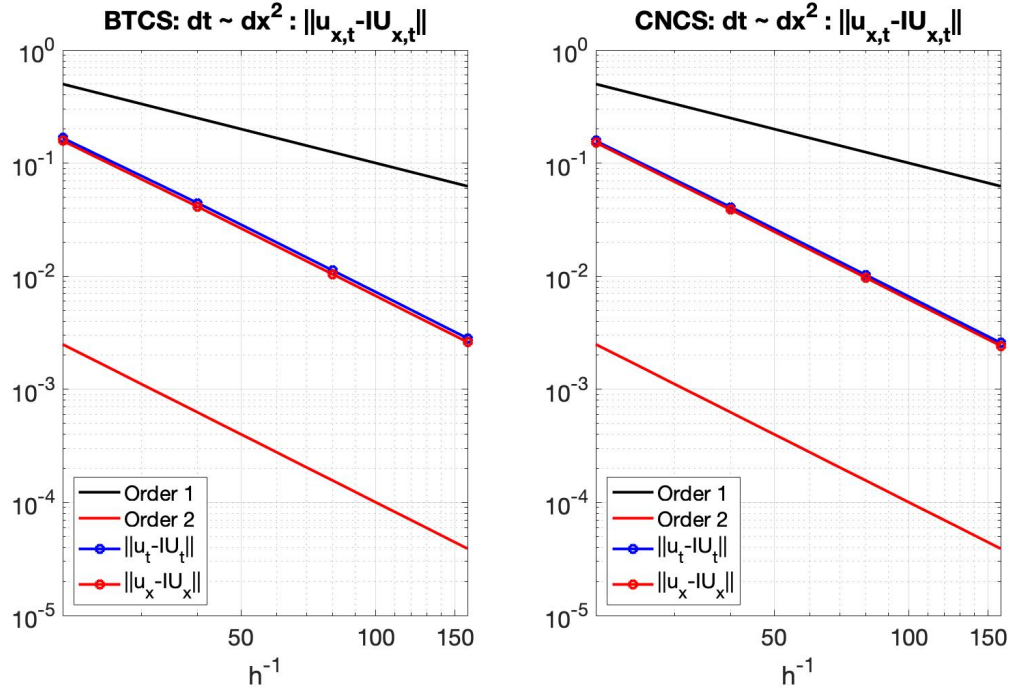
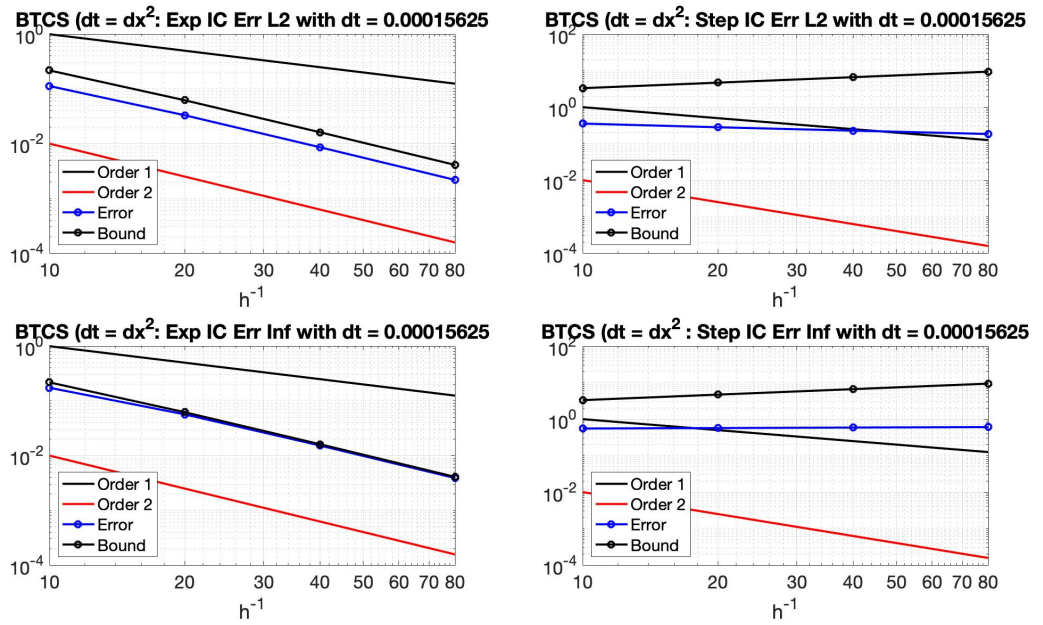
$$u_t = 20(x - 8 - t) \exp(-10(x - 8 - t)^2). \quad (44)$$

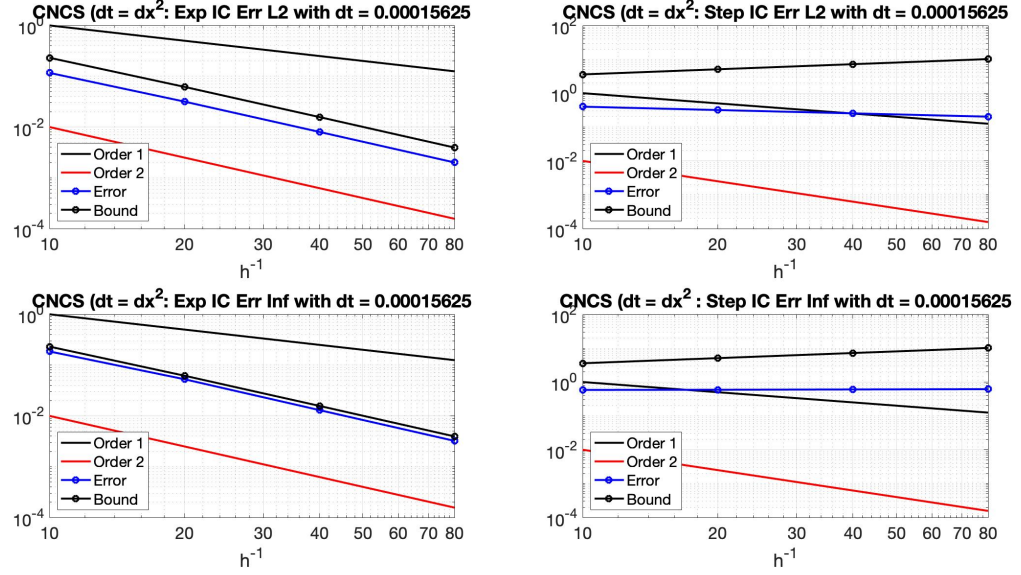
Let us now calculate the order of convergence for $u_x - \mathcal{I}U_x$ in the L_2 norm:

$$\|u_x - \mathcal{I}U_x\|_{L^2((0,L) \times (0,t))} \quad (45)$$

$\mathcal{I}U$ is piecewise linear and hence $\mathcal{I}U_x$ and $\mathcal{I}U_t$ are piecewise discontinuous in the x and t directions respectively. Therefore, we evaluate (24)-(25) at $(t_{i-1/2}, x_{j-1/2})$, where the interpolant derivatives are well-defined for every time-space patch $(t_{i-1}, t_i) \times (x_{j-1}, x_j)$. We then evaluate (43)-(44) at the same point and use numerical integration to calculate (45) approximately:

$$\begin{aligned} \|u_{x,t} - \mathcal{I}U_{x,t}\|_{L^2((0,L) \times (0,t))}^2 &= \int_0^t \|u_{x,t} - \mathcal{I}U_{x,t}\|^2 ds \\ &\approx \sum_{i=1}^{N_t} \Delta t \left(\sum_{j=1}^{N_x} \Delta x ((u_{x,t} - \mathcal{I}U_{x,t})(t_{i-1/2}, x_{j-1/2}))^2 \right). \end{aligned} \quad (46)$$

Figure 3: $\|u_{x,t} - \mathcal{I}U_{x,t}\|_{L^2}^2$ Figure 4: Bound for $dt = dx^2$ with spacings $0.05/2^{2:5}$.

Figure 5: Bound for $dt = dx^2$ with spacings $0.05/2^{2:5}$.

6.2 $u_{x,t} - \mathcal{I}U_{x,t}$ -alternating grid

In this section we look at a grid with alternating spacing. The spacings referenced in the captions is the fine spacing used in each case.

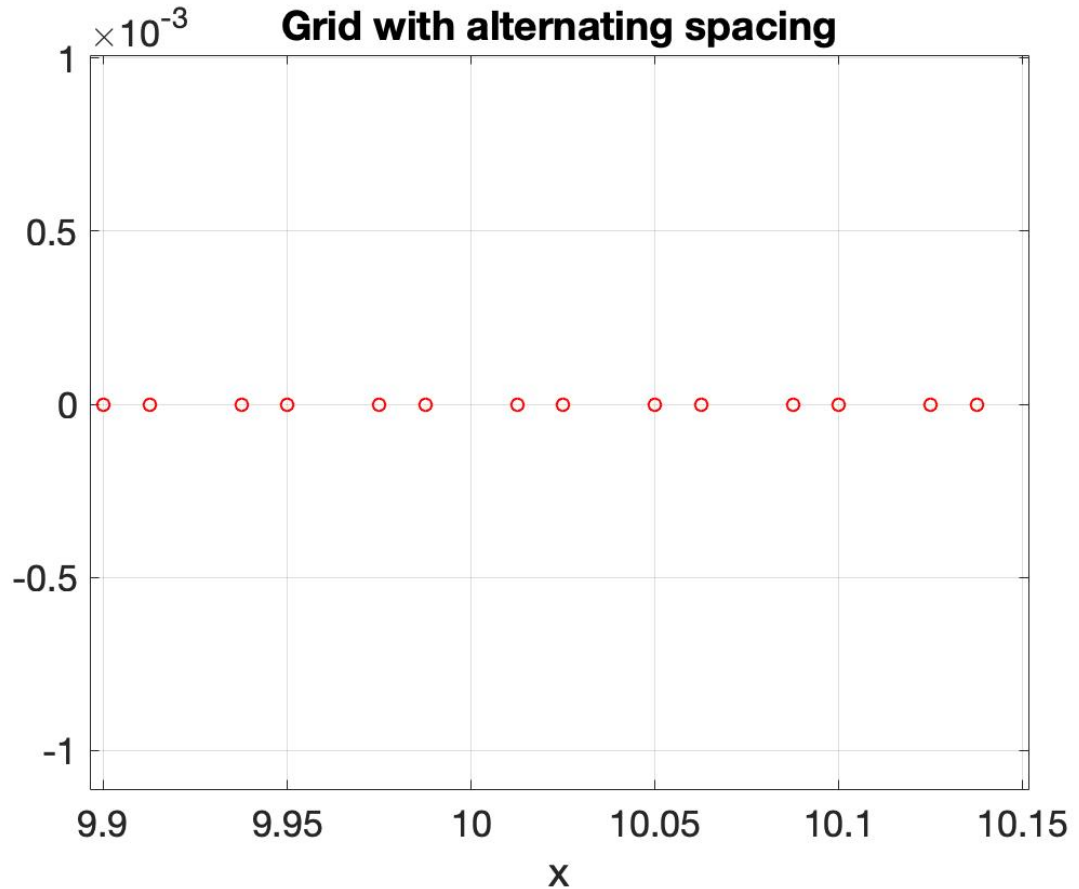
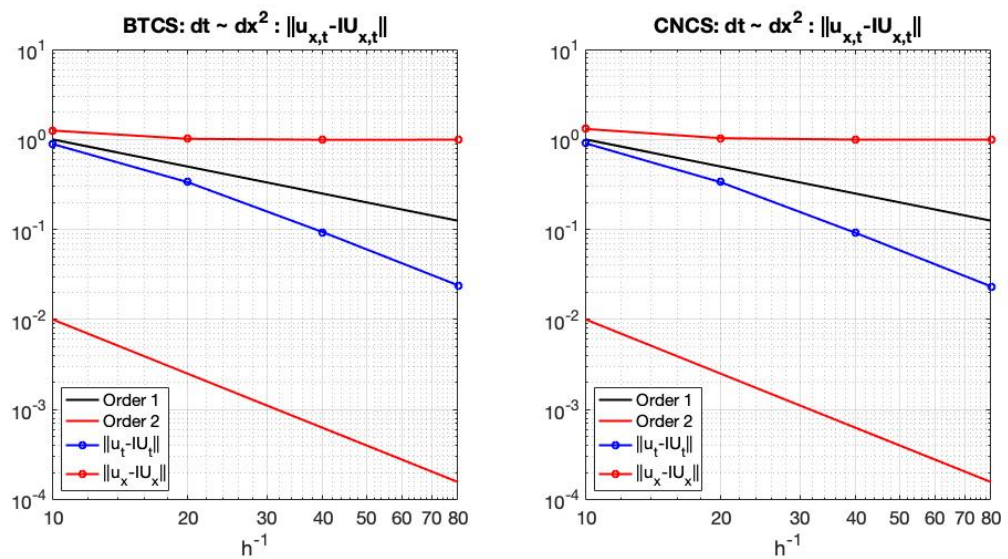


Figure 6: Grid with alternating spacing

Figure 7: alternating spacings $\|u_{x,t} - \mathcal{I}U_{x,t}\|_{L^2}^2$

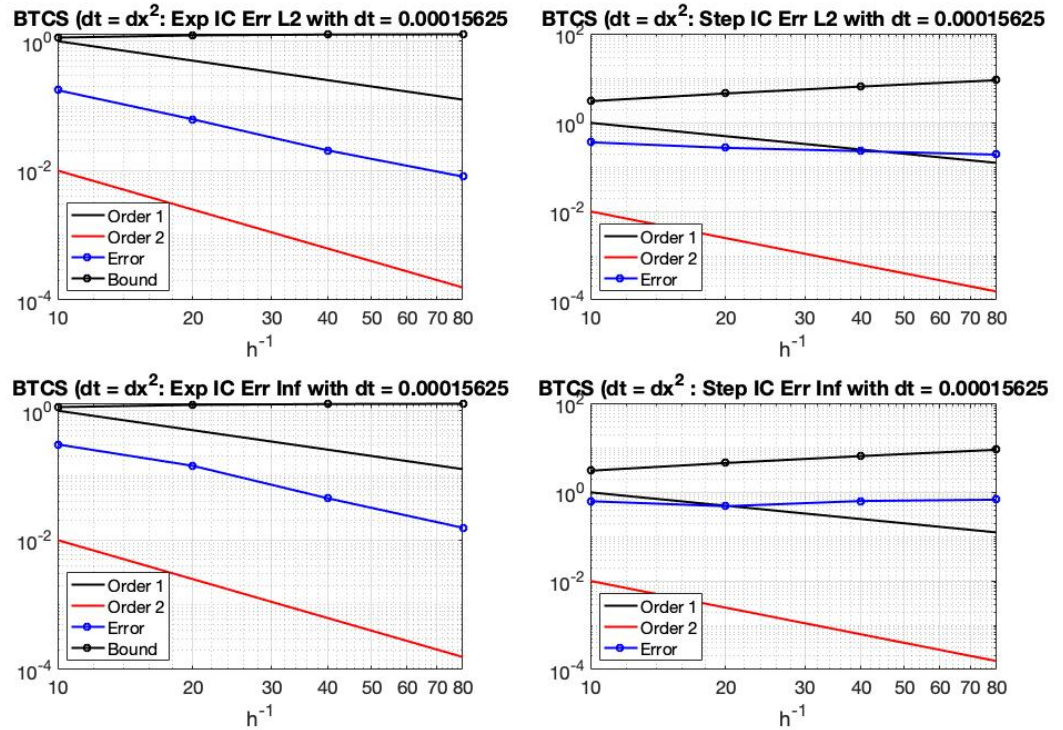
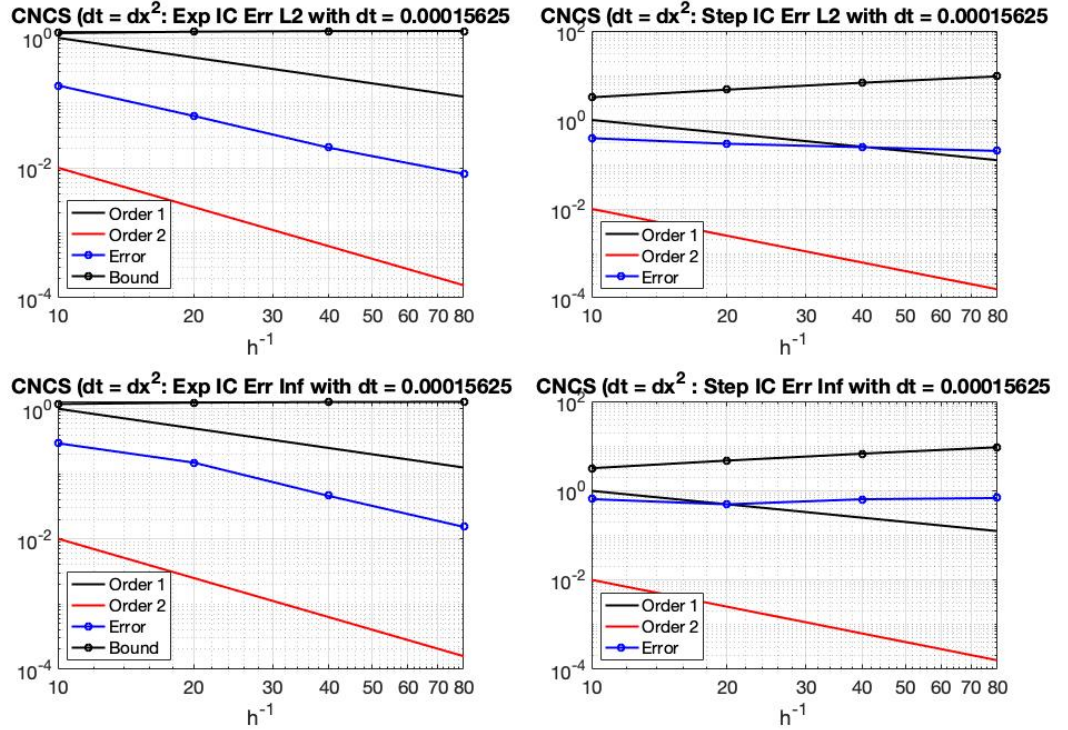


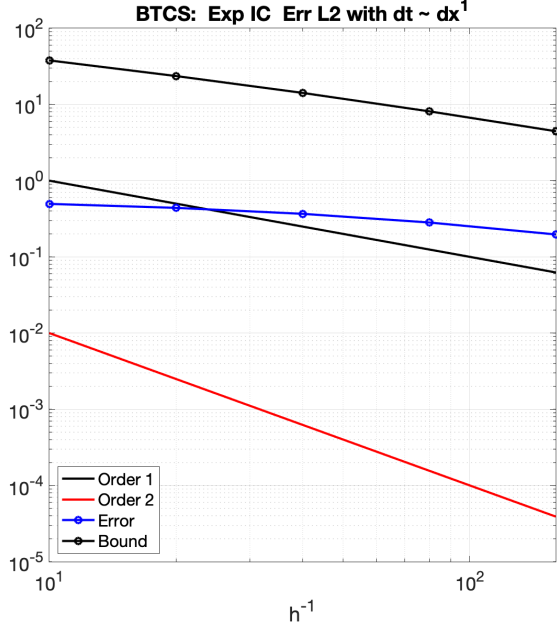
Figure 8: Bound for $dt = dx^2$ with alternating spacings $0.1/2^{0:3}$.

Figure 9: Bound for $dt = dx^2$ with alternating spacings $0.1/2^{0:3}$.

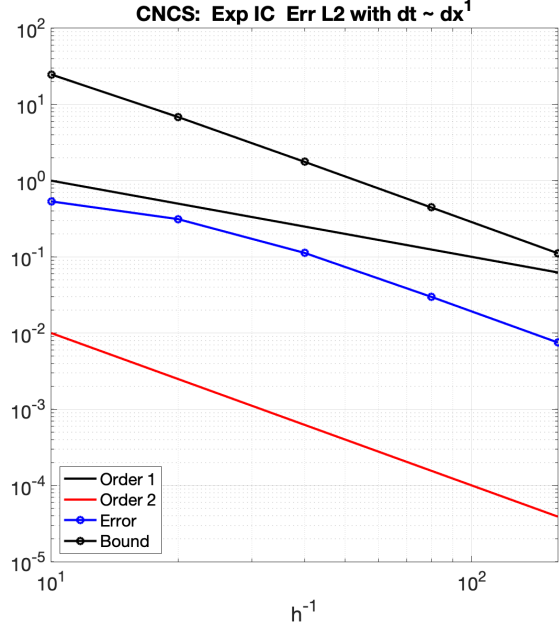
7 Plots by automated code

7.1 Implicit-Smooth

7.1.1 $dt \sim dx^1$



(a) BTCS



(b) CNCS

Figure 10: Plots of the left-hand (blue line with circles) and right-hand (black-line with circles) sides of the square root of (27) with smooth initial conditions given by (40) and a time-step to spatial-step coupling given by $dt \sim dx^1$

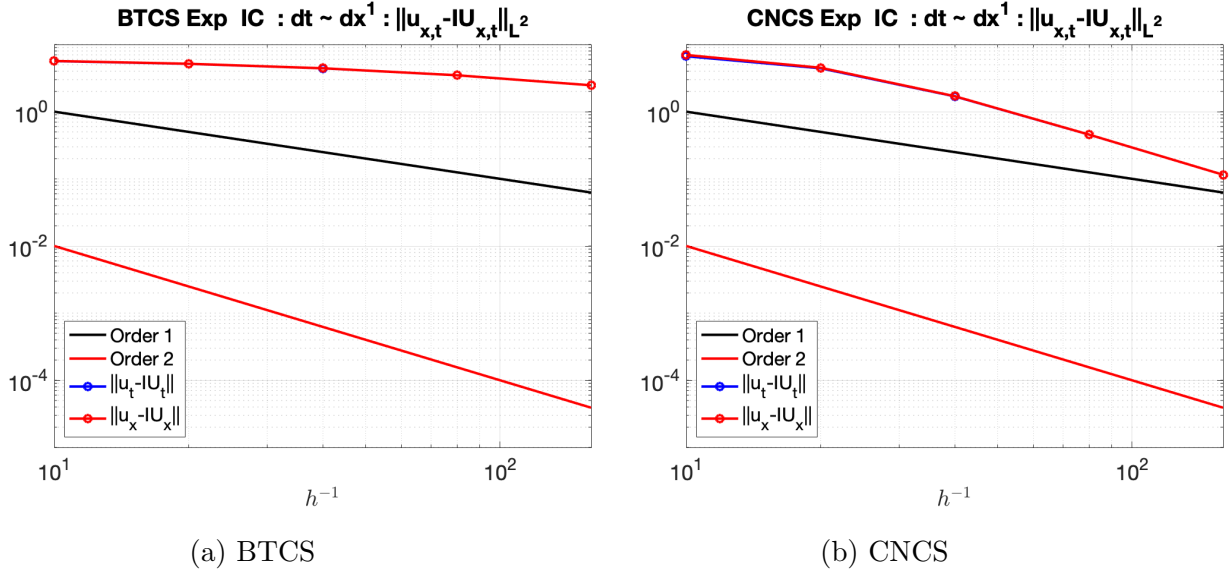


Figure 11: Convergence of the derivatives of the bound to those of the exact solution for smooth initial conditions given by (40) with time-step to spatial step coupling given by $dt \sim dx^1$.

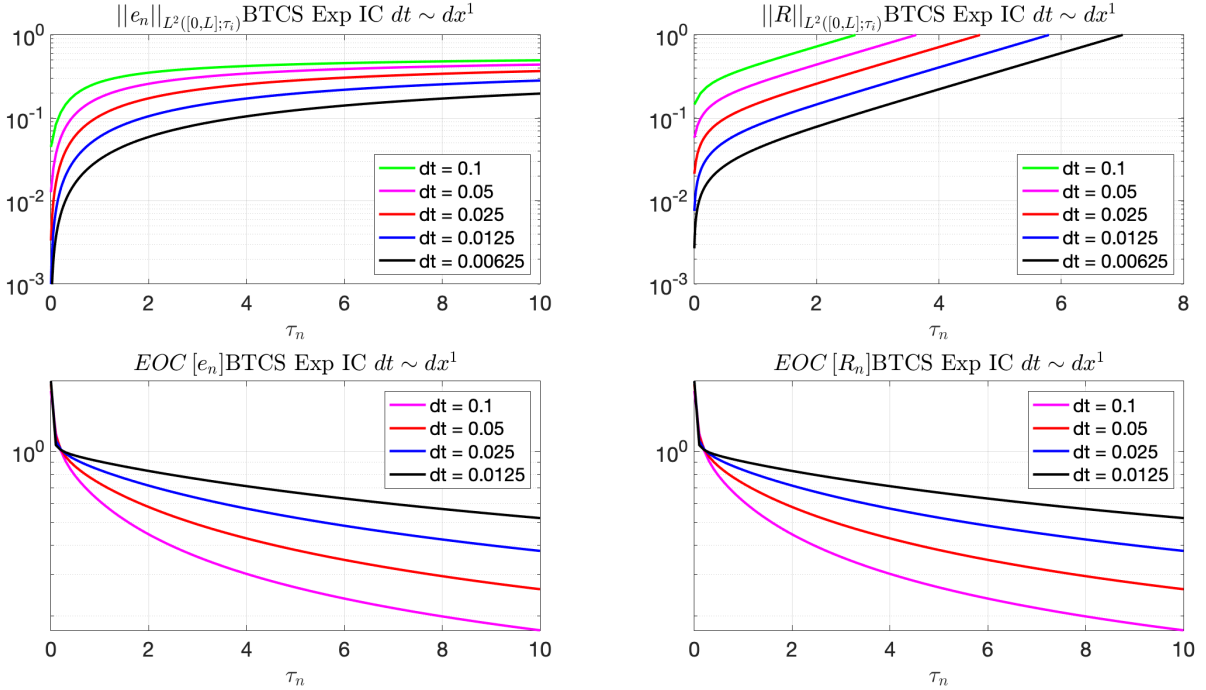


Figure 12: Top row: Evolution of error and bound as given by the left and right hand sides of (27) for BTCS with smooth initial conditions and a time to spatial step coupling $dt \sim dx^1$. Bottom row: Evolution of EOC for the same conditions

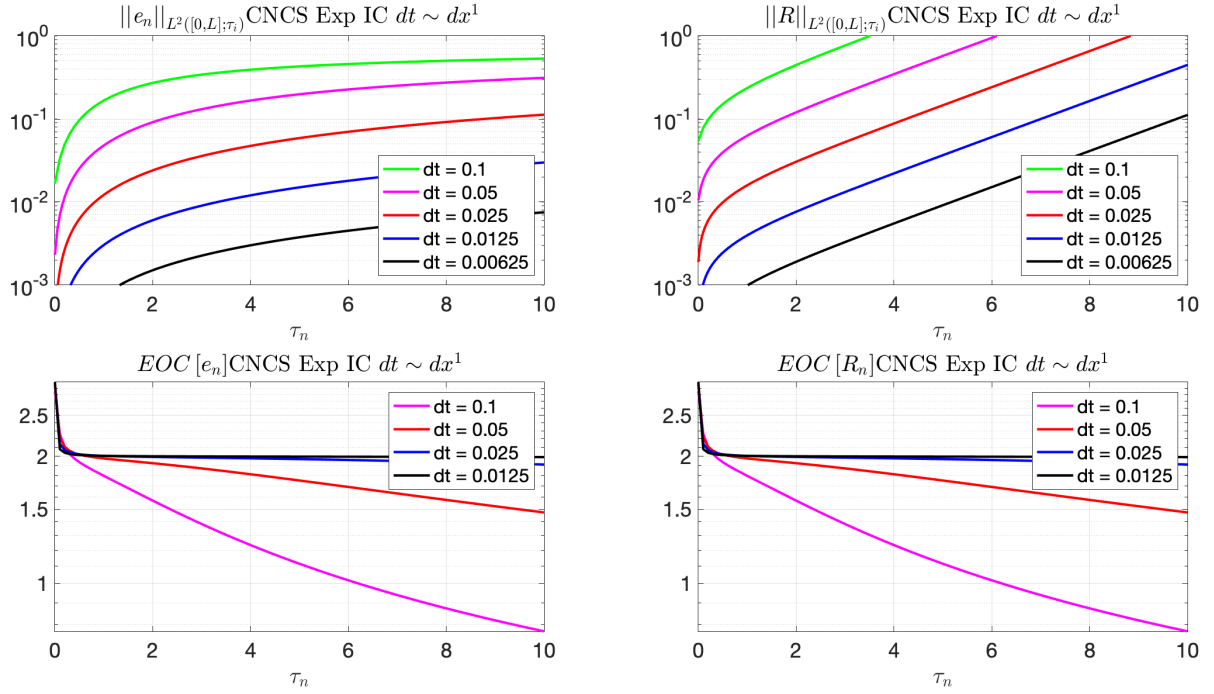


Figure 13: Top row: Evolution of error and bound as given by the left and right hand sides of (27) for CNCS with smooth initial conditions and a time to spatial step coupling $dt \sim dx^1$. Bottom row: Evolution of EOC for the same conditions

7.1.2 $dt \sim dx^2$

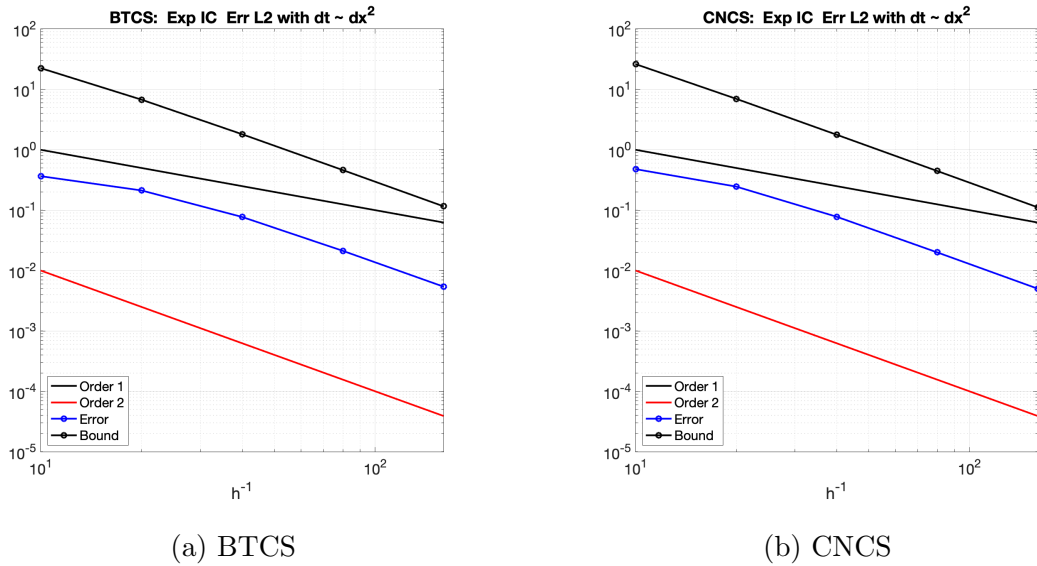


Figure 14: $dt \sim dx^1 L^2$ error at $t = T$ and bound (cumulative)

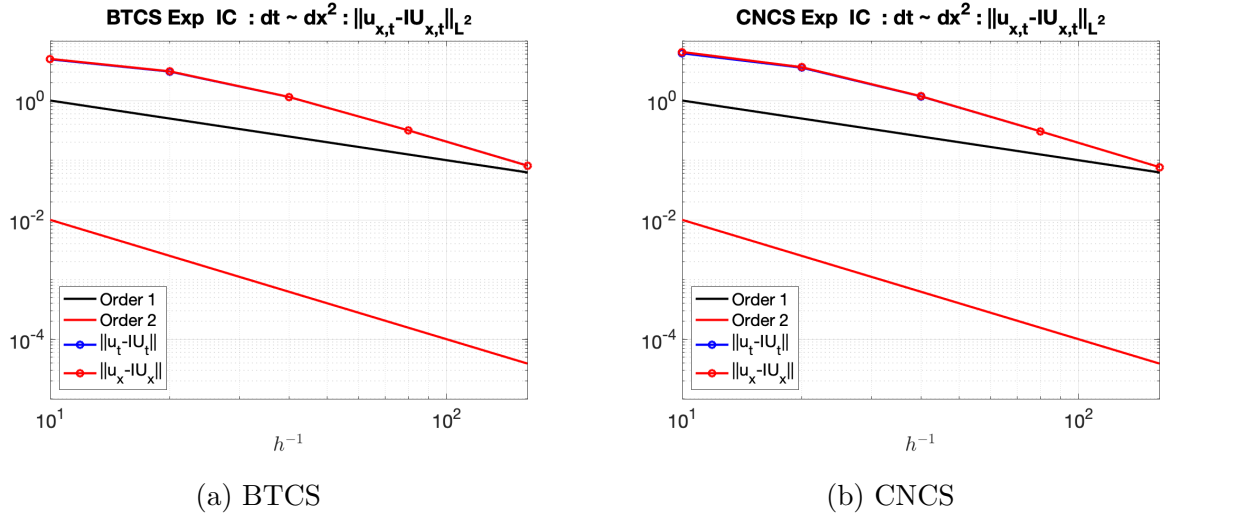


Figure 15: $dt \sim dx^2 \ ||u - \mathcal{I}U||_{L^2}$

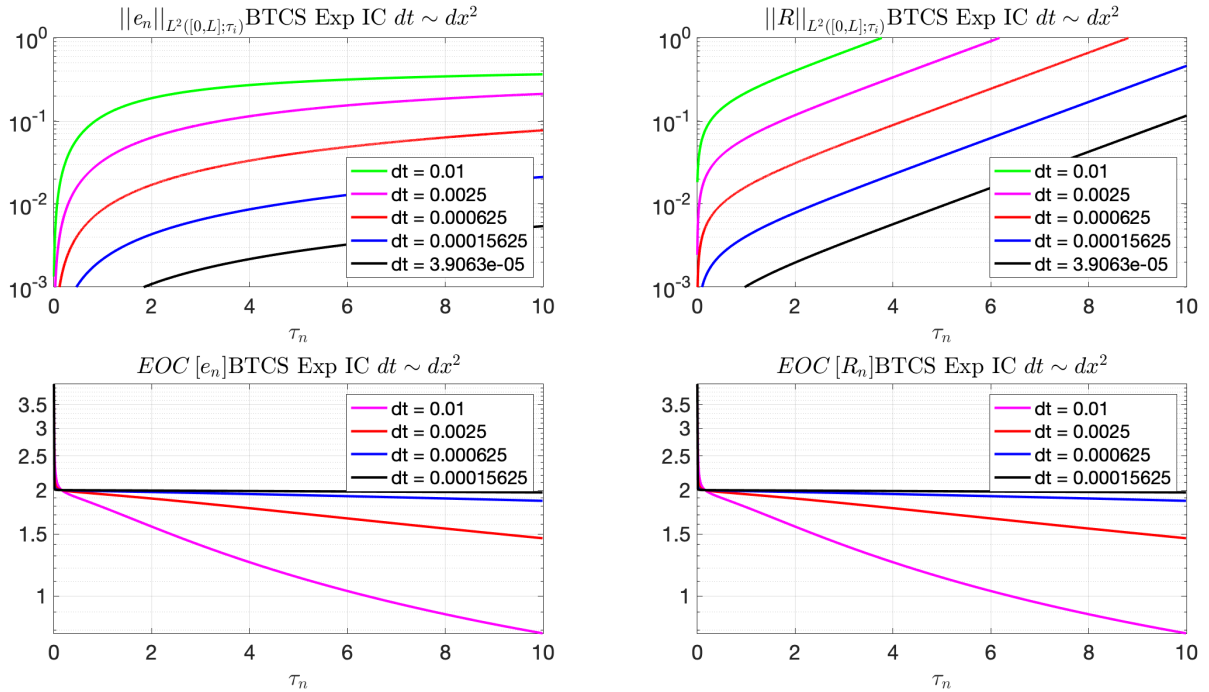


Figure 16: Top row: Evolution of error and bound as given by the left and right hand sides of (27) for BTCS with smooth initial conditions and a time to spatial step coupling $dt \sim dx^2$. Bottom row: Evolution of EOC for the same conditions

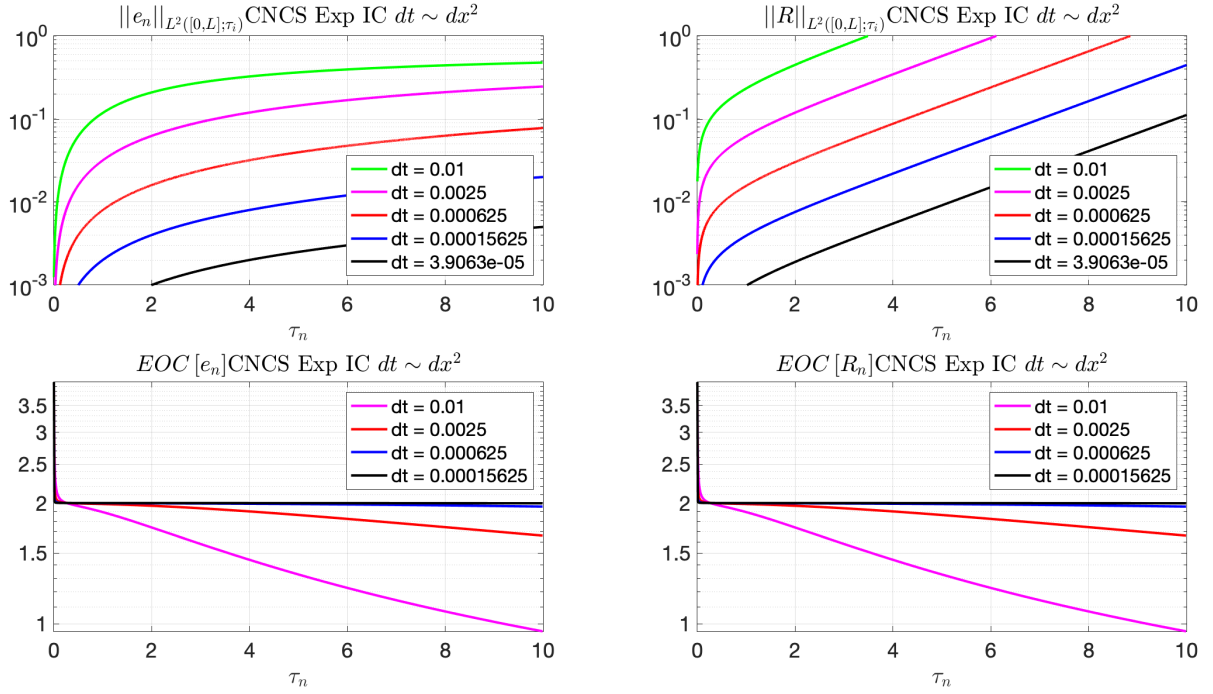


Figure 17: Top row: Evolution of error and bound as given by the left and right hand sides of (27) for CNCS with smooth initial conditions and a time to spatial step coupling $dt \sim dx^2$. Bottom row: Evolution of EOC for the same conditions

8 Implicit-Step

8.0.1 $dt \sim dx^1$

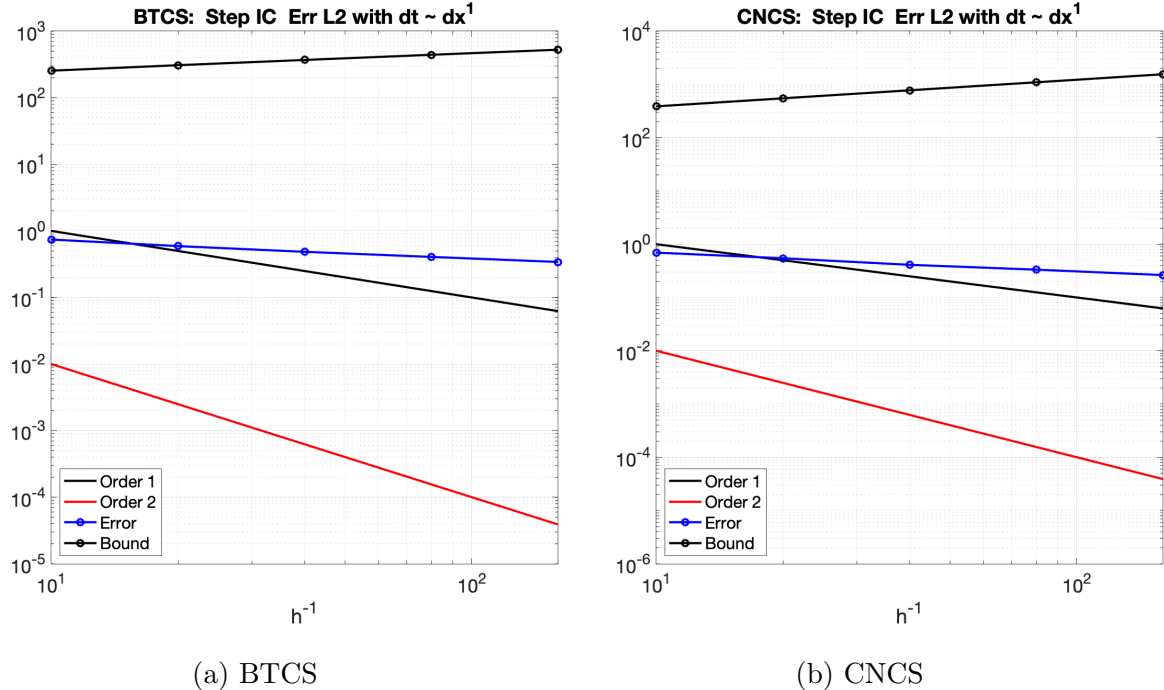
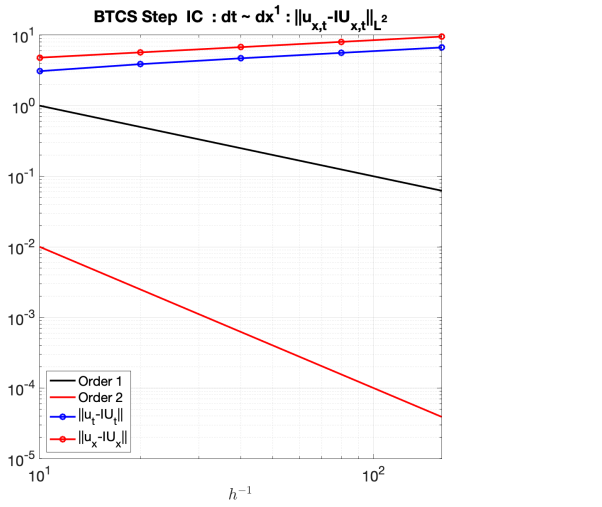
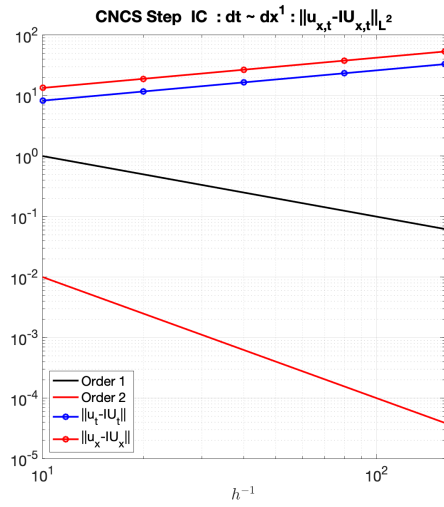


Figure 18: Plots of the left-hand (blue line with circles) and right-hand (black-line with circles) sides of the square root of (27) with step initial conditions and a time-step to spatial-step coupling given by $dt \sim dx^1$



(a) BTCS



(b) CNCS

Figure 19: Convergence of the derivatives of the bound to those of the exact solution for step initial conditions with time-step to spatial step coupling given by $dt \sim dx^1$.

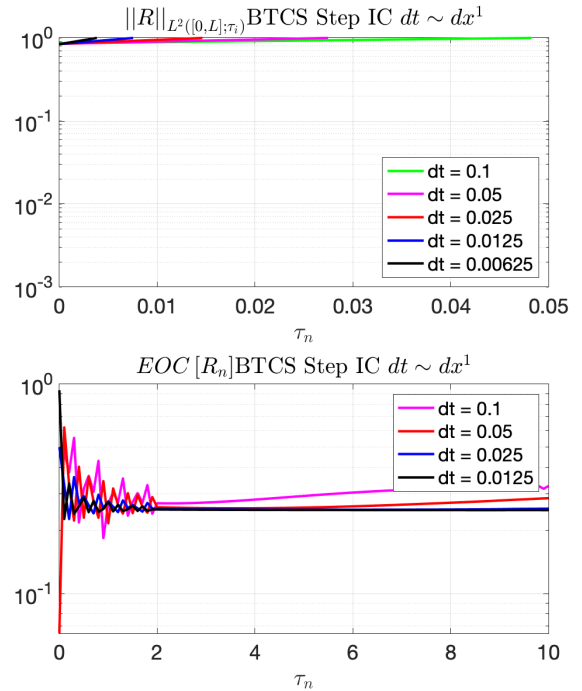
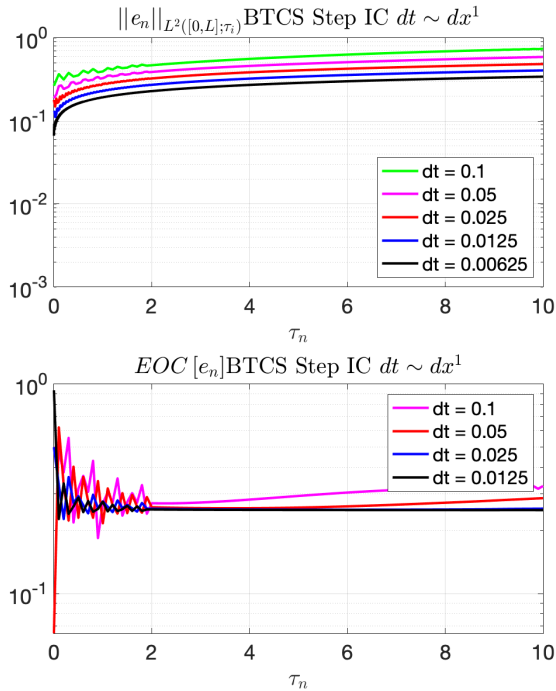


Figure 20: Top row: Evolution of error and bound as given by the left and right hand sides of (27) for BTCS with step initial conditions and a time to spatial step coupling $dt \sim dx^1$. Bottom row: Evolution of EOC for the same conditions

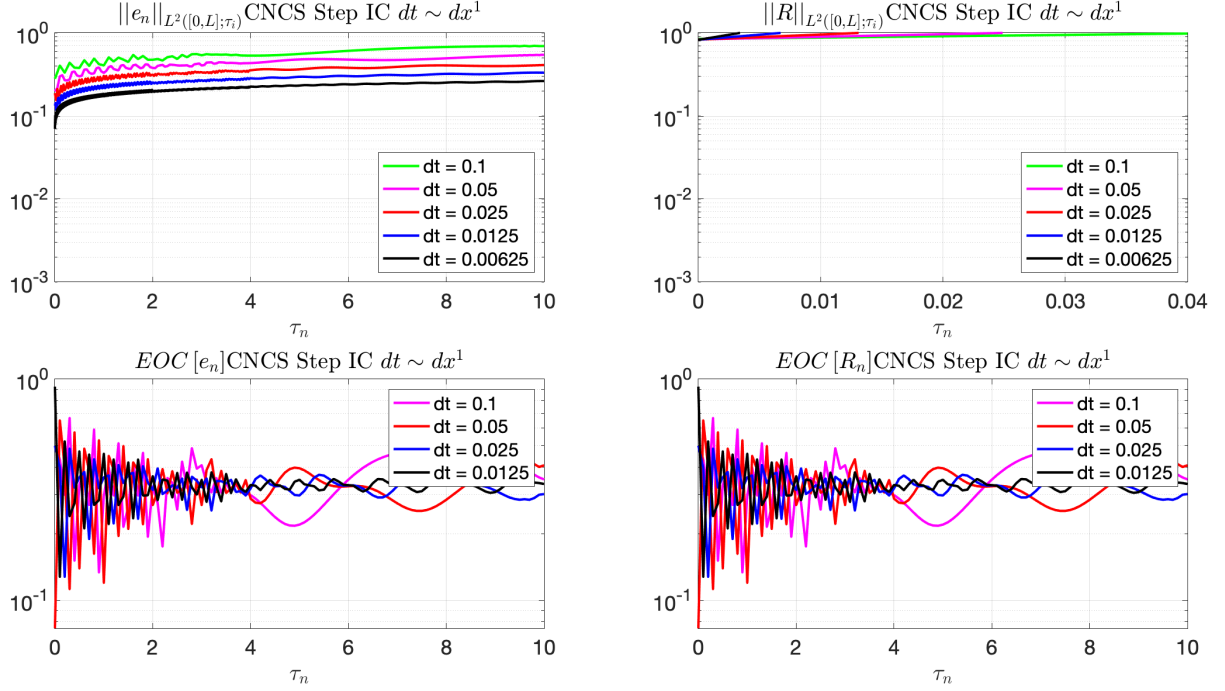


Figure 21: Top row: Evolution of error and bound as given by the left and right hand sides of (27) for CNCS with step initial conditions and a time to spatial step coupling $dt \sim dx^1$. Bottom row: Evolution of EOC for the same conditions

8.0.2 $dt \sim dx^2$

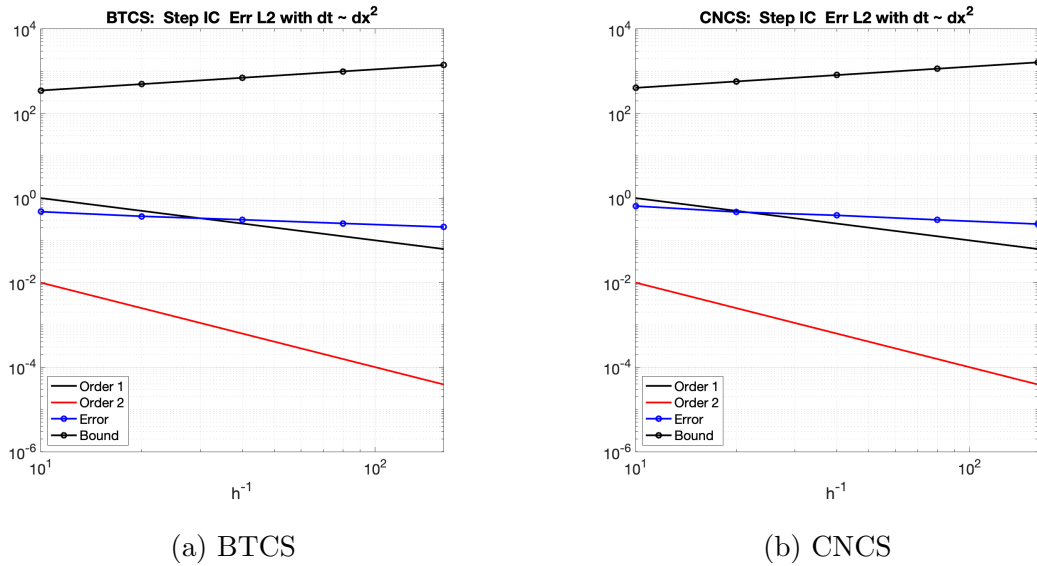
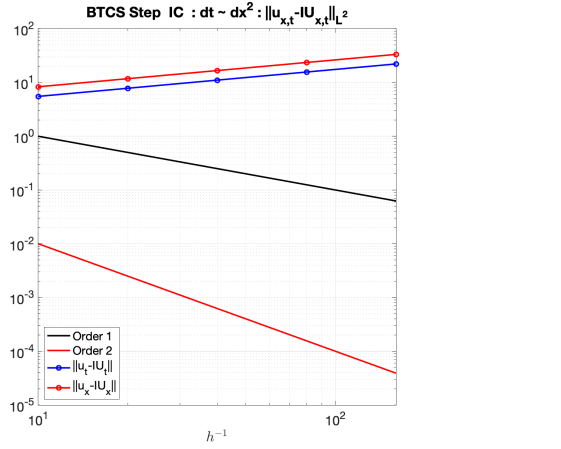
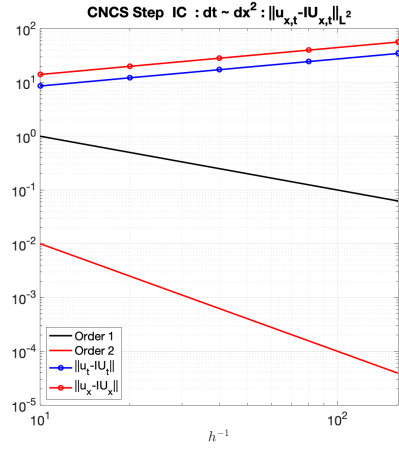


Figure 22: $dt \sim dx^1 L^2$ error at $t = T$ and bound (cumulative)



(a) BTCS



(b) CNCS

Figure 23: $dt \sim dx^2 \ ||u - \mathcal{I}U||_{L^2}$

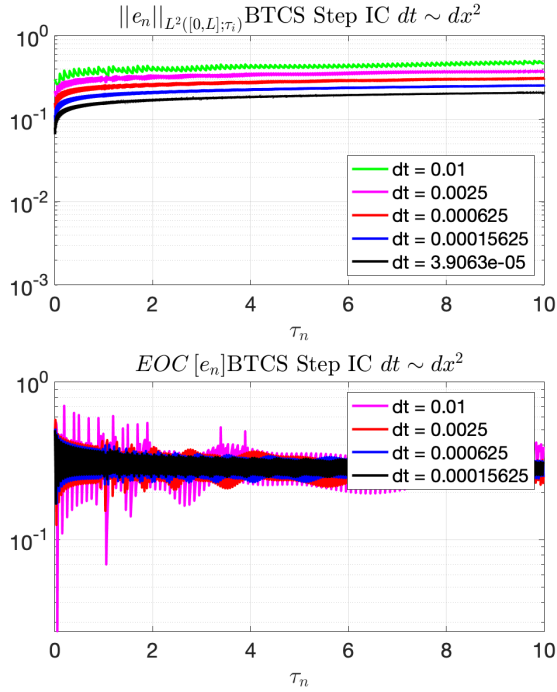
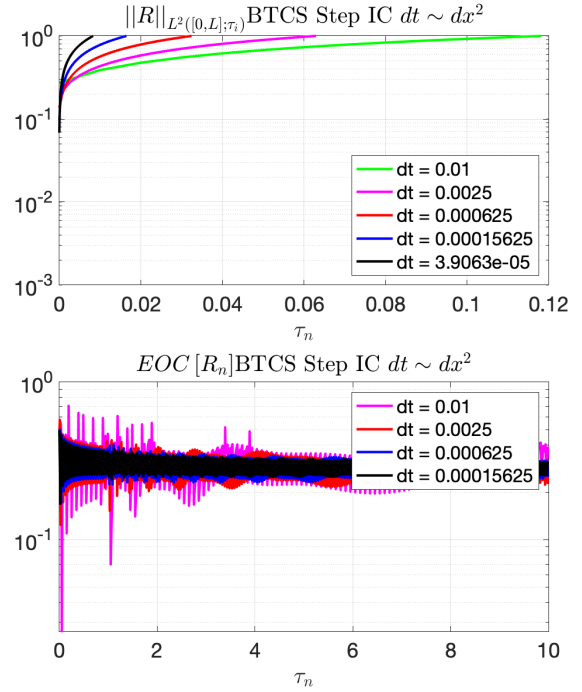


Figure 24: Top row: Evolution of error and bound as given by the left and right hand sides of (27) for BTCS with step initial conditions and a time to spatial step coupling $dt \sim dx^2$. Bottom row: Evolution of EOC for the same conditions



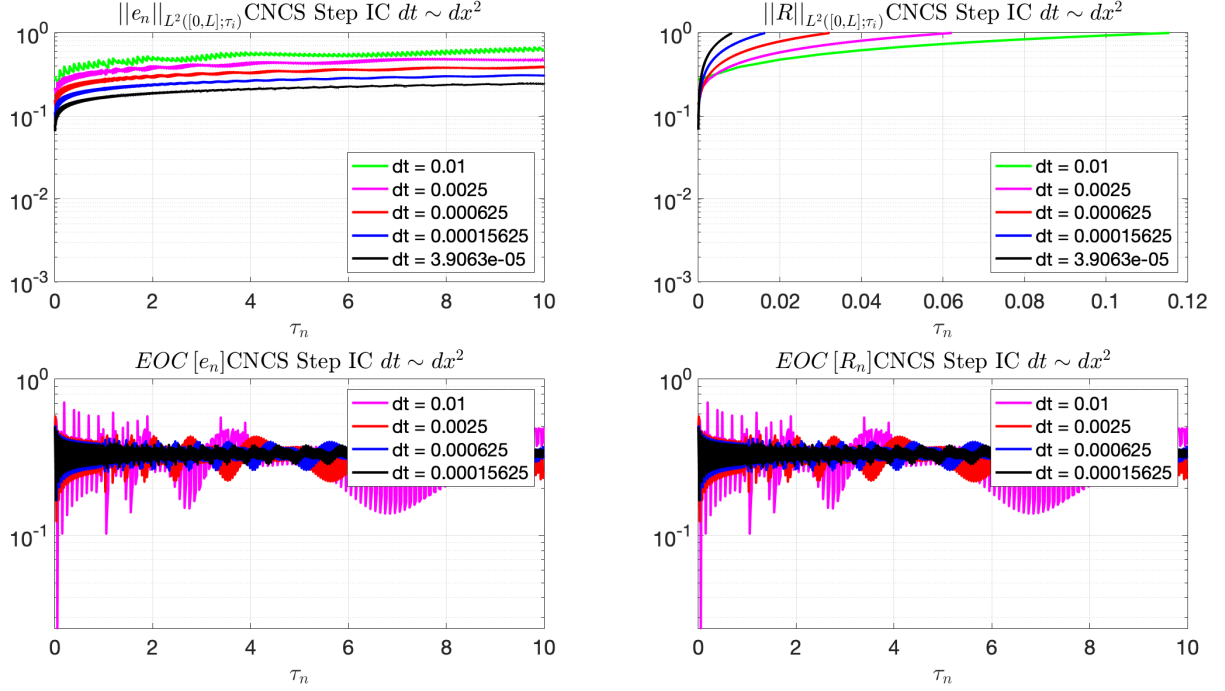
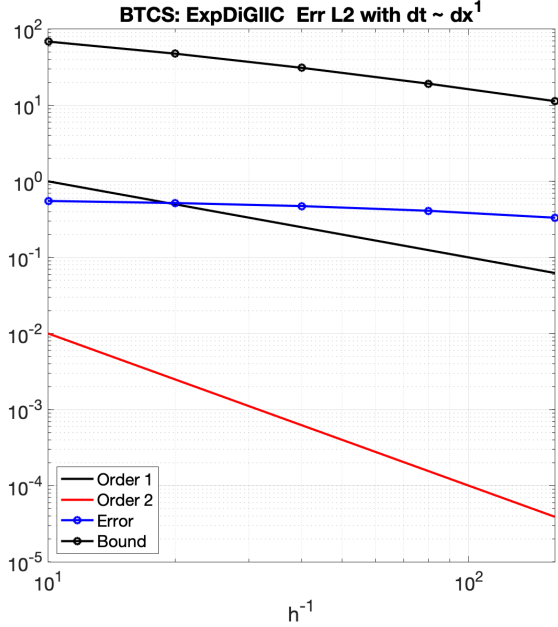


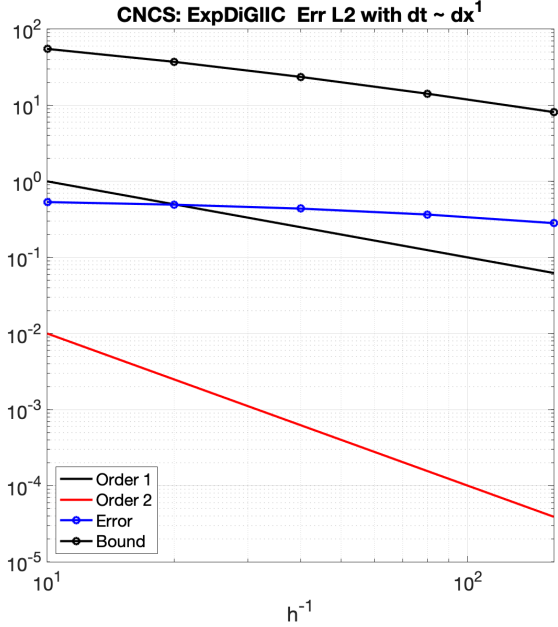
Figure 25: Top row: Evolution of error and bound as given by the left and right hand sides of (27) for CNCS with step initial conditions and a time to spatial step coupling $dt \sim dx^2$. Bottom row: Evolution of EOC for the same conditions

8.1 Implicit-Smooth-diffusion

8.1.1 $dt \sim dx^1$

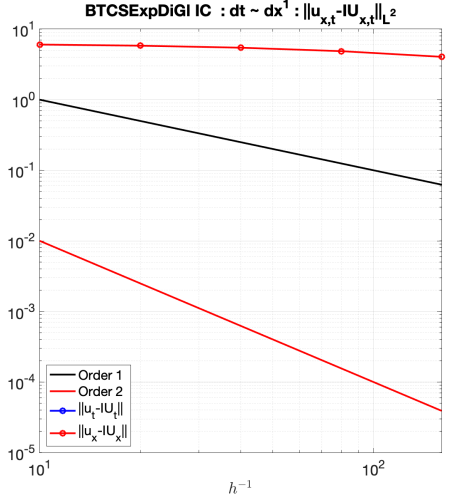


(a) BTCS

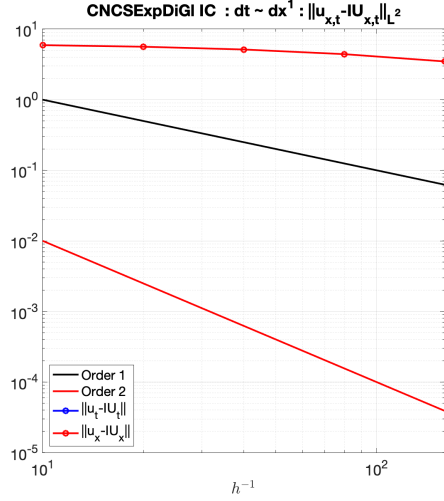


(b) CNCS

Figure 26: Plots of the left-hand (blue line with circles) and right-hand (black-line with circles) sides of the square root of (27) with smooth initial conditions (with global diffusion) given by (40) and a time-step to spatial-step coupling given by $dt \sim dx^1$



(a) BTCS



(b) CNCS

Figure 27: Convergence of the derivatives of the bound to those of the exact solution for smooth initial conditions and global diffusion given by (40) with time-step to spatial step coupling given by $dt \sim dx^1$.

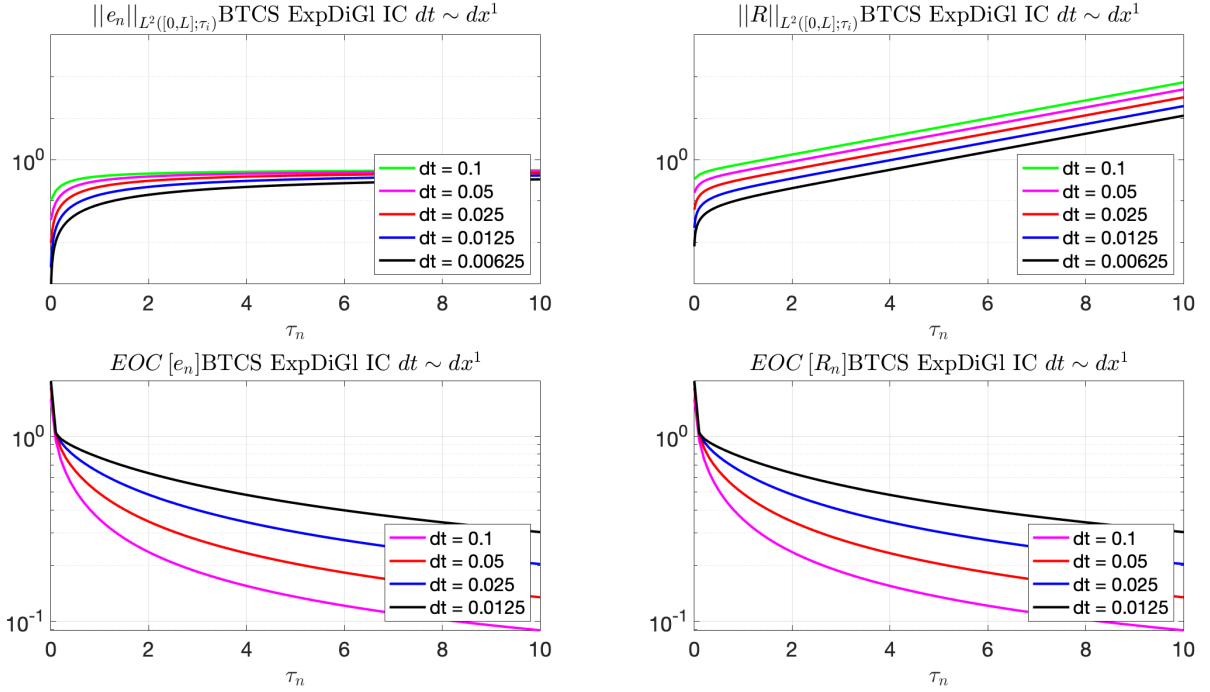


Figure 28: Top row: Evolution of error and bound as given by the left and right hand sides of (27) for BTCS with smooth initial conditions and a time to spatial step coupling $dt \sim dx^1$. Bottom row: Evolution of EOC for the same conditions

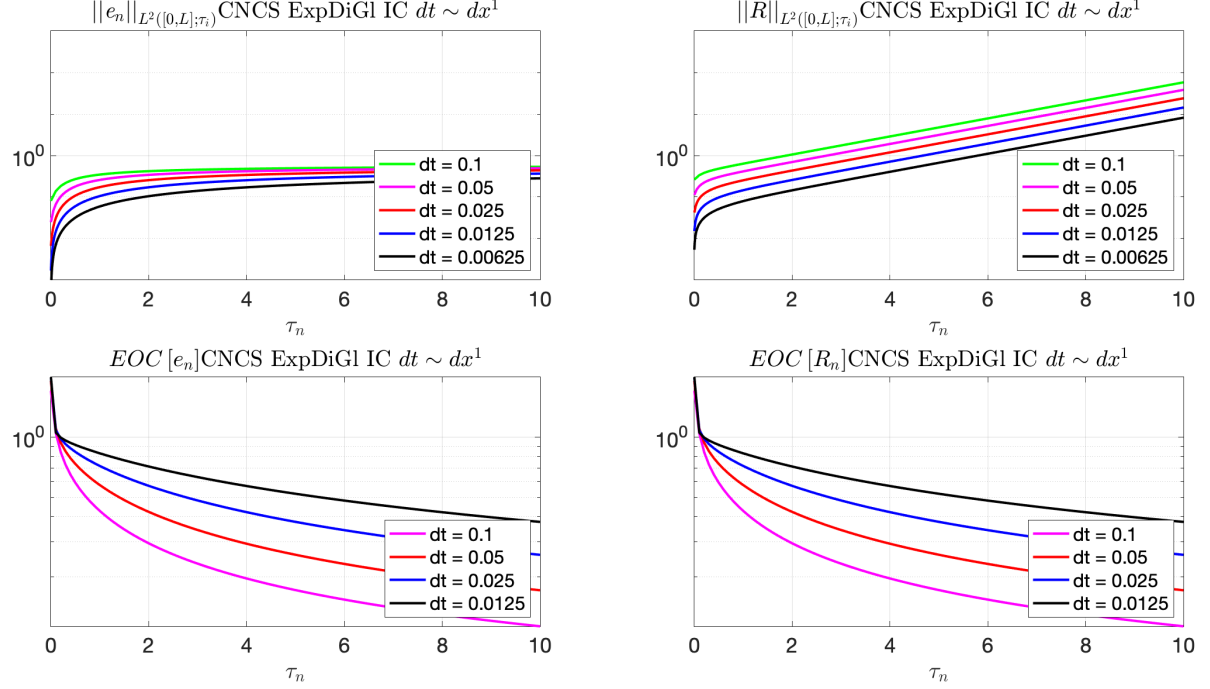


Figure 29: Top row: Evolution of error and bound as given by the left and right hand sides of (27) for CNCS with smooth initial conditions and a time to spatial step coupling $dt \sim dx^1$. Bottom row: Evolution of EOC for the same conditions

8.1.2 $dt \sim dx^2$

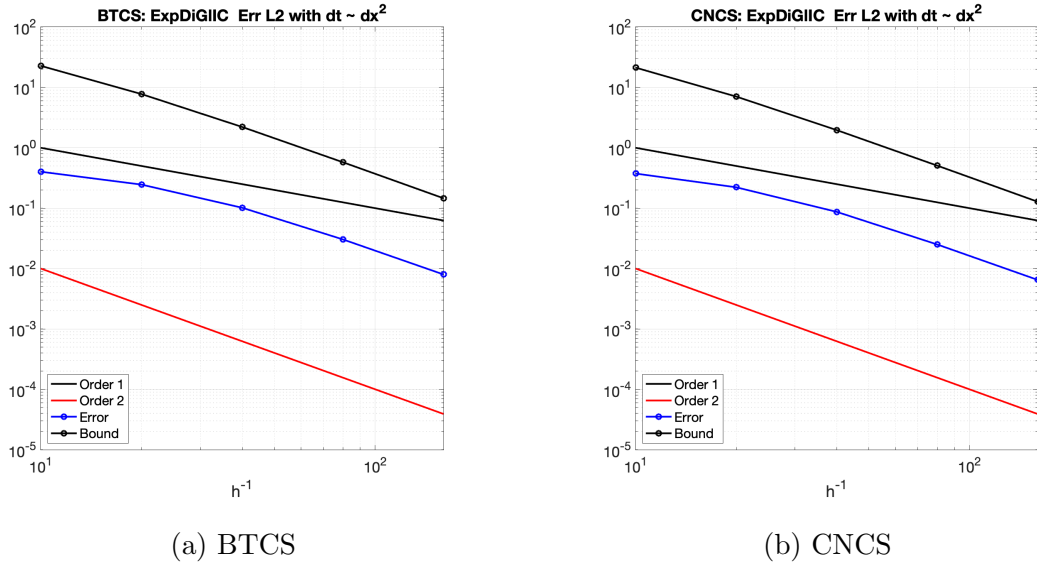
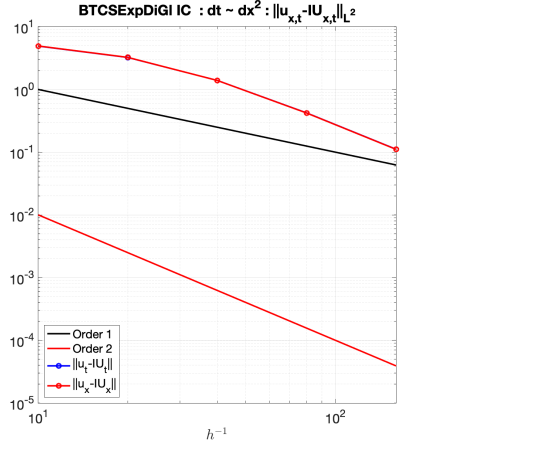
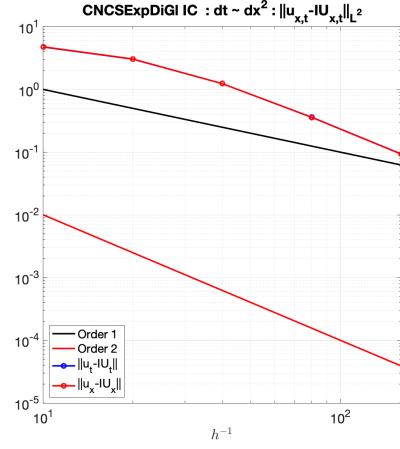


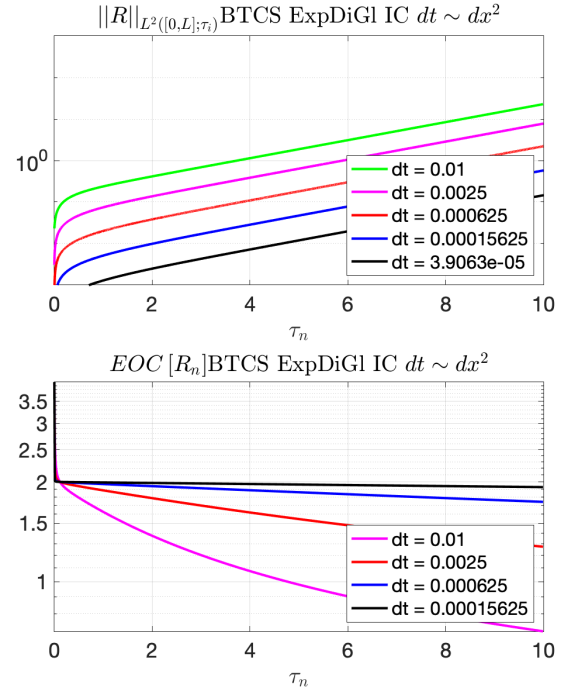
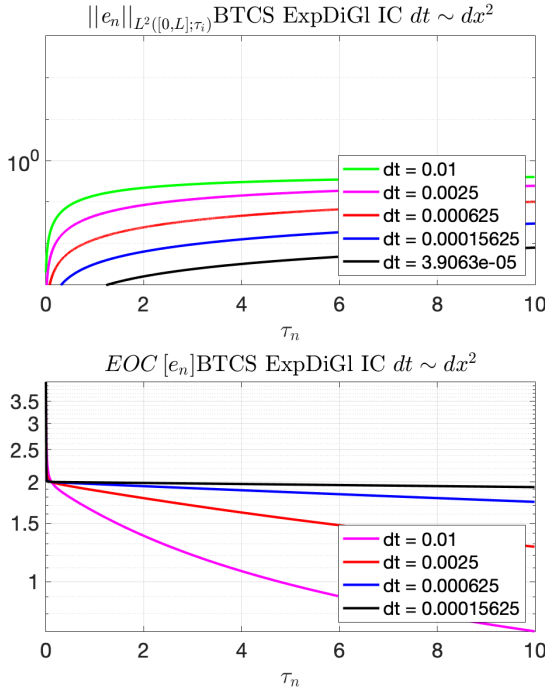
Figure 30: $dt \sim dx^1 L^2$ error at $t = T$ and bound (cumulative)



(a) BTCS



(b) CNCS

Figure 31: $dt \sim dx^2 \|u - \mathcal{I}U\|_{L^2}$ Figure 32: Top row: Evolution of error and bound as given by the left and right hand sides of (27) for BTCS with smooth initial conditions and a time to spatial step coupling $dt \sim dx^2$. Bottom row: Evolution of EOC for the same conditions

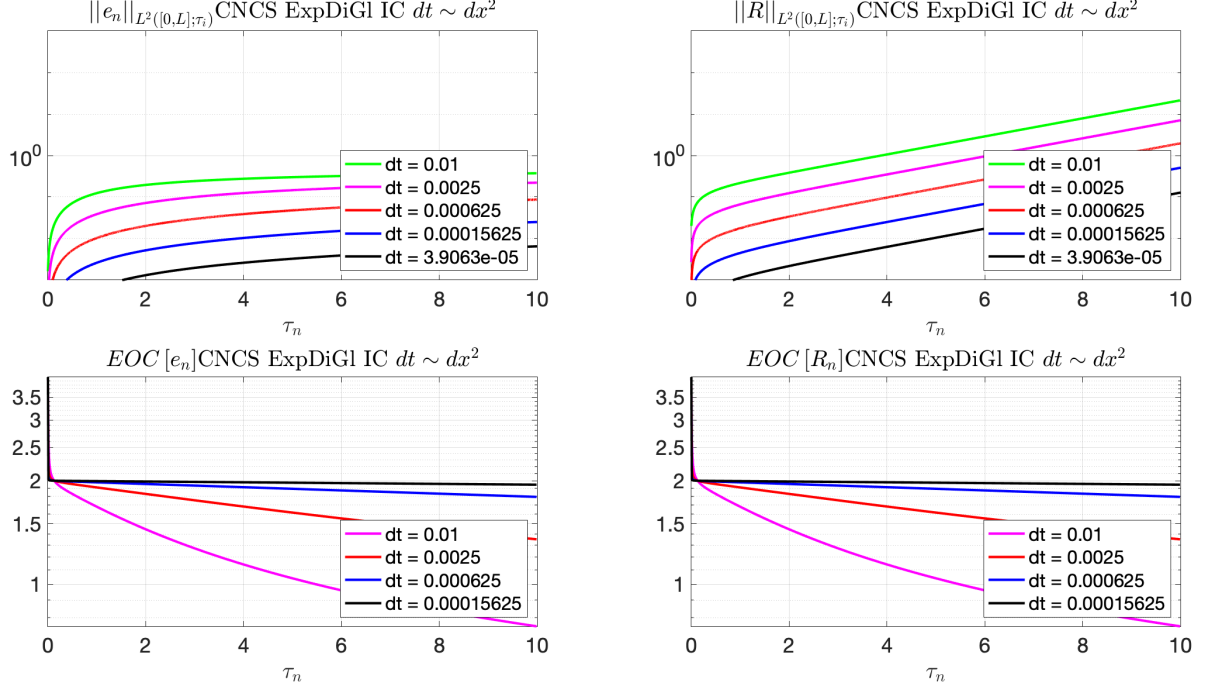
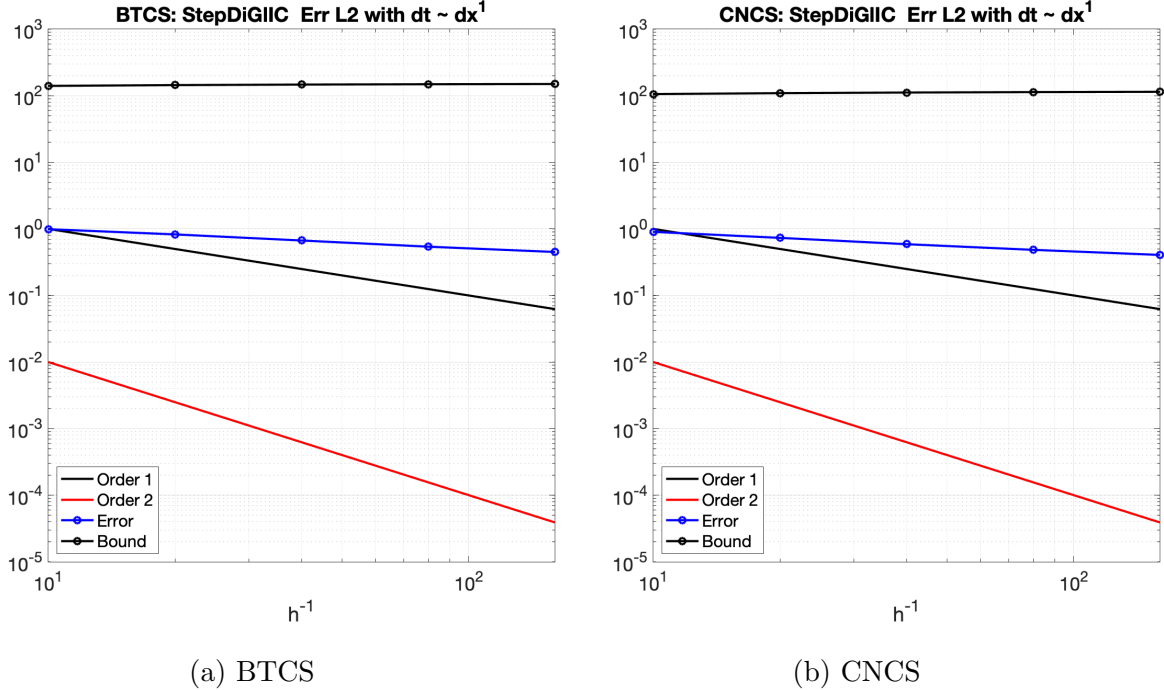


Figure 33: Top row: Evolution of error and bound as given by the left and right hand sides of (27) for CNCS with smooth initial conditions and a time to spatial step coupling $dt \sim dx^2$. Bottom row: Evolution of EOC for the same conditions

8.2 Implicit-Step-diffusion

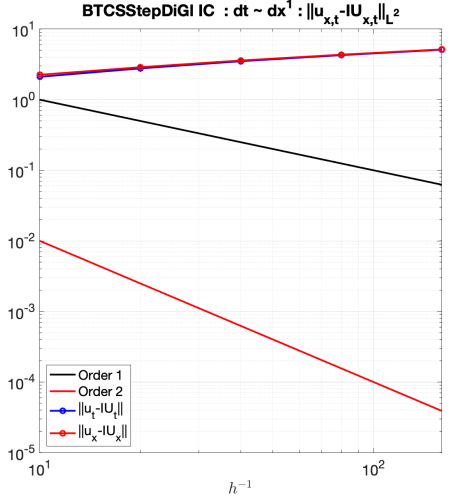
8.2.1 $dt \sim dx^1$



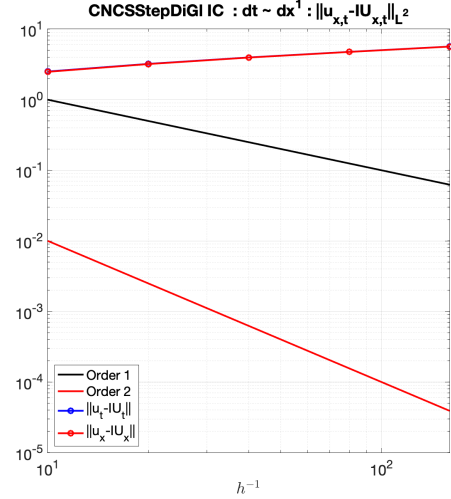
(a) BTCS

(b) CNCS

Figure 34: Plots of the left-hand (blue line with circles) and right-hand (black-line with circles) sides of the square root of (27) with smooth initial conditions (with global diffusion) given by (40) and a time-step to spatial-step coupling given by $dt \sim dx^1$



(a) BTCS



(b) CNCS

Figure 35: Convergence of the derivatives of the bound to those of the exact solution for smooth initial conditions and global diffusion given by (40) with time-step to spatial step coupling given by $dt \sim dx^1$.

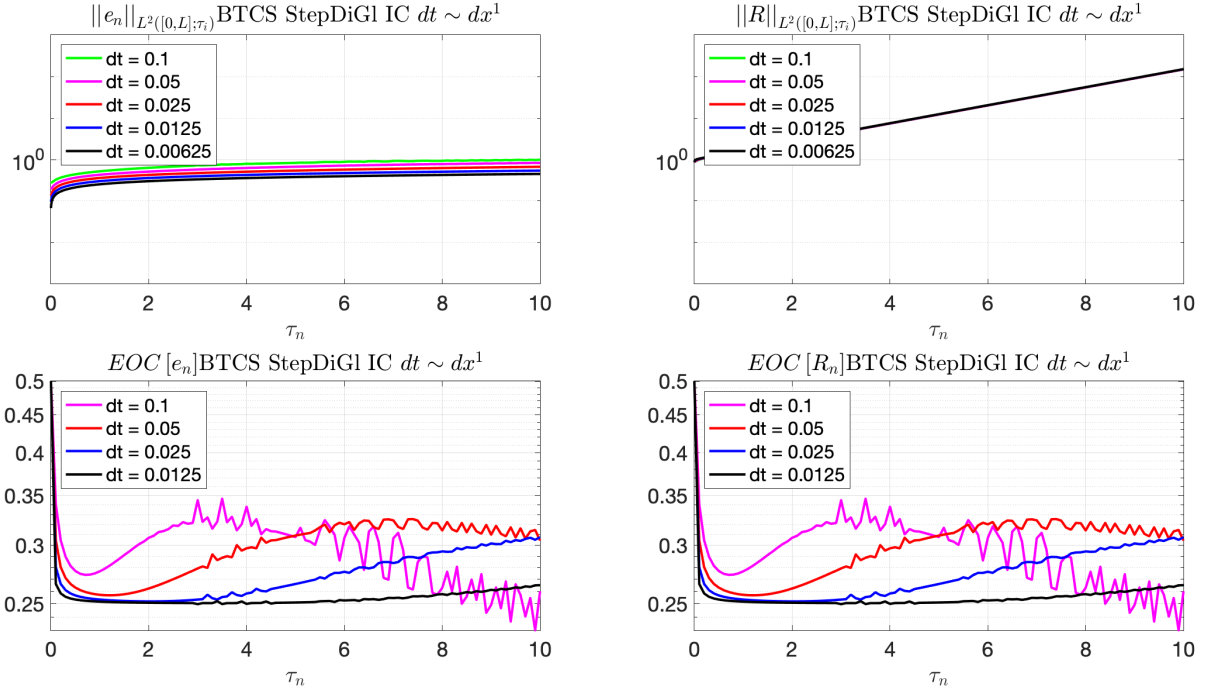


Figure 36: Top row: Evolution of error and bound as given by the left and right hand sides of (27) for BTCS with smooth initial conditions and a time to spatial step coupling $dt \sim dx^1$. Bottom row: Evolution of EOC for the same conditions

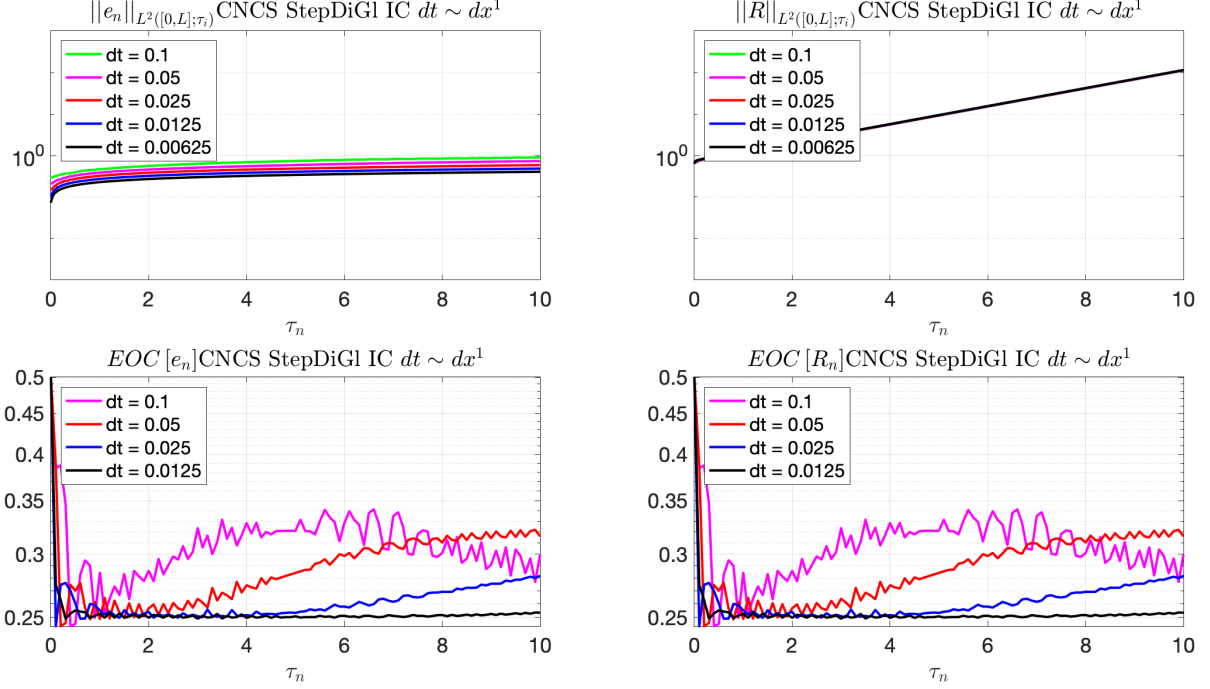


Figure 37: Top row: Evolution of error and bound as given by the left and right hand sides of (27) for CNCS with smooth initial conditions and a time to spatial step coupling $dt \sim dx^1$. Bottom row: Evolution of EOC for the same conditions

8.2.2 $dt \sim dx^2$

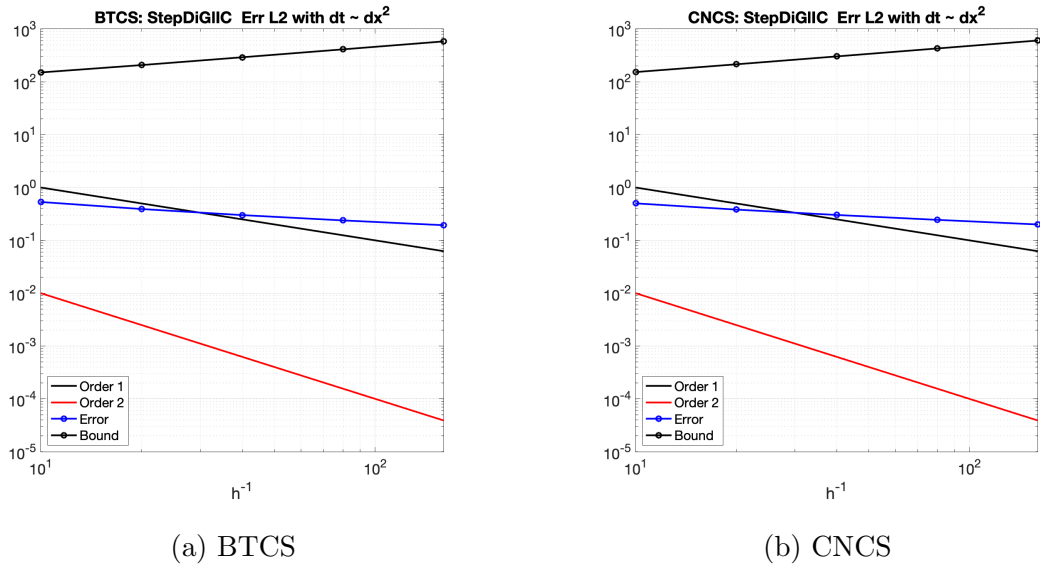
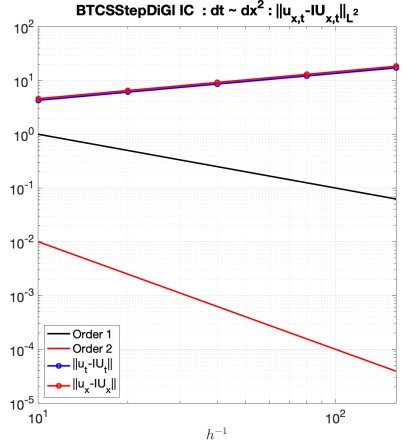
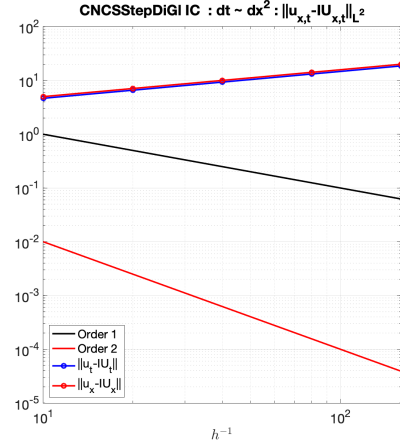


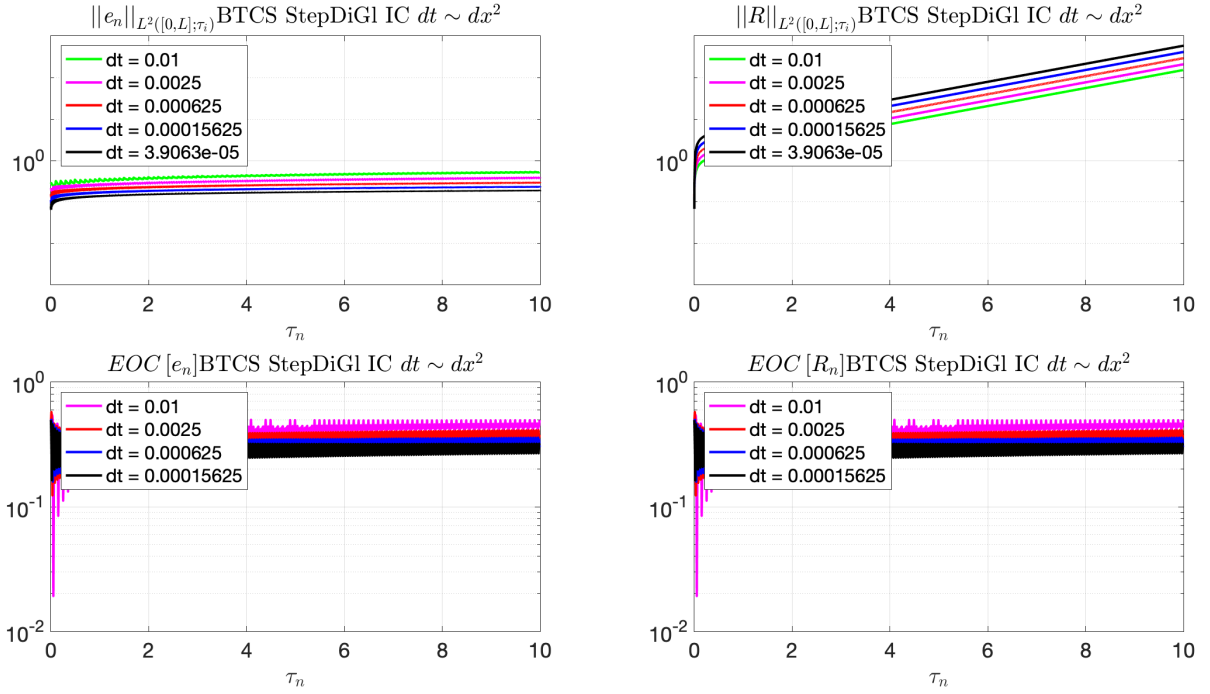
Figure 38: $dt \sim dx^1 L^2$ error at $t = T$ and bound (cumulative)



(a) BTCS



(b) CNCS

Figure 39: $dt \sim dx^2$ $\|u - \mathcal{I}U\|_{L^2}$ Figure 40: Top row: Evolution of error and bound as given by the left and right hand sides of (27) for BTCS with smooth initial conditions and a time to spatial step coupling $dt \sim dx^2$. Bottom row: Evolution of EOC for the same conditions

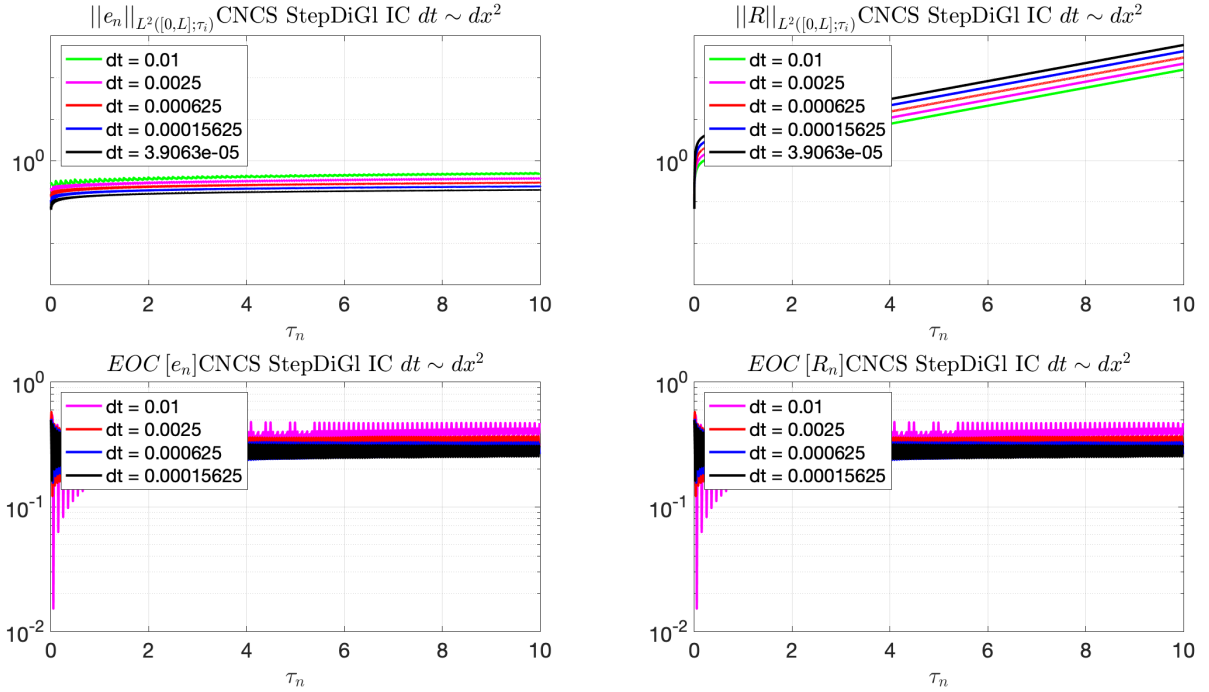


Figure 41: Top row: Evolution of error and bound as given by the left and right hand sides of (27) for CNCS with smooth initial conditions and a time to spatial step coupling $dt \sim dx^2$. Bottom row: Evolution of EOC for the same conditions

References

- [1] R. Vichnevetsky and B. Peiffer, “Error waves in finite element and finite difference methods for hyperbolic equations,” 1975.
- [2] R. Vichnevetsky, “Energy and group velocity in semi discretizations of hyperbolic equations,” *Mathematics and Computers in Simulation*, vol. 23, no. 4, pp. 333–343, 1981.
- [3] R. Vichnevetsky, “Propagation through numerical mesh refinement for hyperbolic equations,” *Mathematics and Computers in Simulation*, vol. 23, no. 4, pp. 344–353, 1981.
- [4] R. Vichnevetsky, “Propagation properties of semi-discretizations of hyperbolic equations,” 1979.
- [5] L. N. Trefethen, “Group velocity in finite difference schemes,” *SIAM review*, vol. 24, no. 2, pp. 113–136, 1982.

- [6] R. Vichnevetsky, “Wave propagation and reflection in irregular grids for hyperbolic equations,” *Applied Numerical Mathematics*, vol. 3, pp. 133–166, 1987.
- [7] J. E. Frank and S. Reich, *On spurious reflections, nonuniform grids and finite difference discretizations of wave equations*. Stichting Centrum voor Wiskunde en Informatica, 2004.
- [8] D. Long and J. Thuburn, “Numerical wave propagation on non-uniform one-dimensional staggered grids,” *Journal of Computational Physics*, vol. 230, no. 7, pp. 2643–2659, 2011.